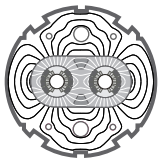

LHC Project Note 422

July 15, 2009

Energy deposition in LHC MB magnet and quench threshold test with beam.

Bernd Dehning, Agnieszka Priebe, Mariusz Sapinski *
CERN CH-1211 Geneva 23, Switzerland

Keywords: superconducting magnets, quench prevention

Summary

In this study a particle shower development in the Main Dipole magnet due to the losses of the LHC beam particles is simulated with Geant4 Monte Carlo code. The signals observed in Beam Loss Monitors located outside the magnet cryostat are related to the energy deposited in the magnet coil. The beam abort thresholds in the Beam Loss Monitors corresponding to quench-provoking temperature increase of the magnet coil are determined. This thresholds depend on the beam energy, loss duration and the loss dimension. The results of the simulations are compared with the first and the second beam-induced quench of the Main Dipole.

*mail: mariusz.sapinski@cern.ch

Contents

1 Introduction

The Main Dipole (MB) is the most abundant magnet on the Large Hadron Collider [1]. The total number of 1232 of these superconducting magnets with magnetic length of about 14.3 meters each are installed around the machine. They induce maximum field of 8.33 Tesla in the center of the vacuum chamber. This field allows to keep protons of 7 TeV on the orbit.

The Beam Loss Monitoring [2] system is designed measure the beam losses which could damage the accelerator components and trigger the beam dump sequence. It will also protect the superconducting magnets from losses which would lead to quenches, i.e. transitions of the magnets coil from superconducting to resistive state.

The quench phenomena has been extensively studied (see for instance [3]). For the purpose of this study it is important to distinguish two stages of quenching. A quench precursor is a local transition of the cable (or a fraction of the cable) to resistive state. It can be detected by the Quench Protection System (QPS) [4, 5], which measures the voltage difference on the cable. The quench precursor, depending on the heat load parameters, can develop into quench, when the whole cable irreversibly changes to resisitive state, or can disappear. The typical decision time after which the cable state is superconducting again or resistive is of the order of miliseconds. If the head load is such that the quench precursor will not develop into quench but it still generates a voltage difference with value and duration above predefined thresholds, it will trigger the quench heaters and quench the whole magnet. Therefore in the following the "beam-induced quench" definition is extended to the situations where the transition of the magnet to the resistive state is due to QPS decision.

Because of a high magnetic field and high nominal current the MB magnet is one of the LHC magnets most fragile to quenches. The enthalpy density limit of the cables for the transient losses, when the heat transfer along the cable and from the metal to helium is negligible, varies from about 31.3 mJ/cm^3 for injection energy to about 0.9 mJ/cm^3 for collision energy [6]. In case of steady state losses, when the energy evacuation from the coil reaches a constant value, the maximum power which can be transferred to cryogenic system without quenching the magnet is about 320 mW/cm^3 for injection and 12 mW/cm^3 for collision energies [7, 8]. For the losses of intermediate duration various algorithms are proposed [7, 9].

The Main Dipole magnets are less exposed to the beam losses than the lattice quadrupole magnets (MQ) due to smaller betatron function and a smaller orbit excursion. Therefore typically there are no Beam Loss Monitors installed on the MB magnets, while six of them are installed on or in the vicinity of every MQ magnet. There are a few exceptions from this rule, usually in the Straight Sections of the machine, mainly due to specific needs of ion beam [10] and when the dipoles are positioned downstream of the collimators in the cleaning insterion where the off-momentum protons are deviated and can be lost. In these cases the BLM monitors are installed on MB magnets. This study deals with the special cases because the first experimental data from the beam-induced quenches were collected on monitors

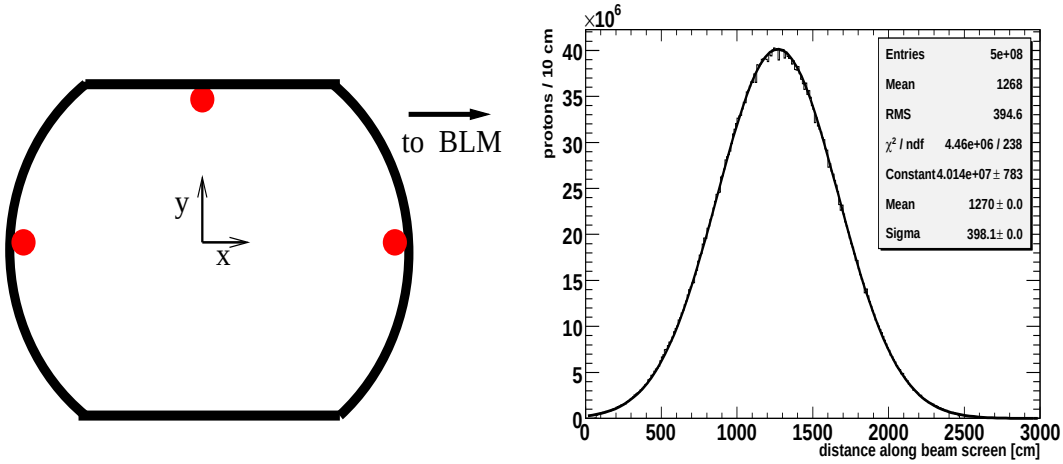

Figure 1: *Left plot: schematic view of location of simulated beam losses on the beam screen. Right plot: results of a calculation showing the distribution of the lost protons along the beam screen due to impact of single bunch with transverse* $\sigma_{\mathrm{beam}} = 1$ mm *and containing* $4 \cdot 10^9$ *protons. The impact angle is* 240 μrad.

attached to Main Dipoles.

The main goal of this study is determination of the quench-protecting thresholds for the BLMs placed on the MB magnet. Therefore the particle shower simulation has been performed in order to determine relation between energy deposition in the magnet coil and signal outside the cryostat. No particular loss scenarios as wrong collimator settings or creation of a local beam bump, have been considered here. The results of the simulation has been verified with the data taken during the first two beam-induced quenches. This comparison gives a first benchmark for the method of the BLM threshold settings. The outcome of this study, especially of the comparison of the simulated signals with the one measured during the quench events, is applied to thresholds set on BLMs protecting other cold elements of the LHC.

2 Geometry and simulated events

The model of MB magnet has been implemented in Geant4. It includes essential elements of the magnet such as beam screen, cold bore, coil, collar, yoke, thermal insulation and the cryostat. The concrete tunnel walls and the rock behind them are simulated as they play an important role in thermalization of neutrons. In total the geometry consists of about 200 Geant4 volumes.

The coil is described as made of uniform mixture of Copper (59.2%), Niobium (19%), Titanium (16.8%) and Liquid Helium (5%). The density is found to be 7.78 g/cm^3. The terminations of the magnet, where the coils are bend and the

helium vessel is closed at the ends, are also included in the simulated geometry, even if in this report only the losses contained within the magnet length are analysed. The losses in vicinity of magnet interconnections are analysed elsewhere [11].

Three beam loss locations are analysed. They are depicted on the left plot of Figure 1 and are called horizontal left and right and vertical upward loss. In each position about 1000 lost protons have been simulated for beam energies between 250 GeV and 8 TeV. The Geant4 in version 9.0 patch 01 has been used. The choice of physics list is based on comparisons done in [15] and the list called QGSP_BERT_HP is used. This list combines Quark-Gluon String (QGSP) modelling of hadron interaction at energies above 12 GeV with Bertini parametrization of the hadronic cascade below 10 GeV and with High Precision neutron transport (containing the resonant interactions with nucleai). In the intermediate energy range (10-12 GeV) a parametrized model derived from GEISHA [16] is used. The protons impact on the beam screen with the angle of 240 μrad or, in special case of second quench (Section 10), 750 μrad.

The cascade develops initially in the beam screen, cold bore and in the coil. The interaction length of the stainless steel which is the beam screen and the cold bore material is $\lambda_{\mathrm{steel}} = 170.4$ mm. Therefore, about 90% of protons entering the beam screen with angle of 240 μrad initiate the cascade there. The rest interact in the cold bore. In case of the impact angle increased to 750 μrad this proportions change and 50% of protons go throught the beams screen.

The coil material has the nuclear interaction length similar to beam screen material with $\lambda_{\mathrm{NbTiCu}} = 167.7$ mm. In the coil the energy deposits are registered in cells with length of 4.7 cm and with azimuthal size of about 4°. In the radial direction the internal coil is divided in three layers with radial dimension of 0.512 cm each. The mininal volume of the bin is therefore 0.517 cm^3. This size of the bins have been chosen to fit the shape of the hadron cascade.

The BLMs on the real MB magnet are 50 cm long cylinders located on the cryostat every 2 to 5 meters. Here, in order to investigate the shape of the signal outside the cryostat, the particles are registered in two long cylinders on both sides along the magnet. Here they are called beam-1 BLM and beam-2 BLM. The cylinders are divided into 50 cm segments which correspond to actual ionisation chamber longitudinal dimension [1]. These segments are called BLMs and the central position is given. For instance BLM at 75 cm means section positioned between 50 and 100 cm from the loss location. It must be stressed that in such geometry the impact of the particles which in reality enter the BLM volume from endcups is neglected. The error made due to this choice of the geometry is small because the bulk of the particles enter BLM with large angles.

The simulation has been performed with 1 mm cut on secondary particles range. This translates to, for example, a 1.2 MeV cut on electron energy in the coil. It has been found that the results are statistically important for at least 10^4 lost protons for injection energy and 2000 lost protons for collision energy, where the showers provide more particles outside the cryostat. These are the numbers of protons in

[1] The discussion of the BLM active volume is in Section 7

various samples considered.

The simulation has been performed on **lxbatch** cluster at CERN and typical time needed to simulate one proton was about 30 minutes.

3 Magnetic field map

The magnetic field map has been obtained using ROXIE [17], a program for magnetic field calculations inside the magnets. The map mesh step is 5.1 mm and between the mesh points a linear interpolation of field values is used.

The map is two-dimensional, what means that it does not take into account the field configuration at the magnet terminations. Only transverse components of the magnetic field are used. In order to avoid unphysical field change, in the termination zones where the coil is bended, the field is made to change smoothly to zero.

The field map is presented on upper plot of Figure 2 for the magnet yoke. Inside the coil the maximum field is reached on the inner surface of the inner coil. The field inside the coil is shown on bottom plot of Figure 2.

4 Stability margin

The stability margin is the maximum amount of energy which can be deposited in a volume of the magnet coil without quenching. For the fast transient losses (below 100 μs[2]) which are mainly considered here, the deposited energy has no time to dissipate out of the cable strands which are made of the superconductor filaments in a copper matrix. Therefore the stability margin is defined by the enthalpy limit ($\mathrm{H_{strand}} = \mathrm{H_{strand}(T_{quench})} - \mathrm{H_{strand}(1.9K)}$): a difference between strand enthalpy at operational temparature of 1.9 K and critical tempearture at which quench occures. Reaching this enthalpy limit in a small fraction of the coil might lead to a creation of a quench precursor which could heal by itself, but this kind of quench, as it has been shown by experience on real magnets (Sections 9 and 10), triggers the Quench Protection System heaters and finally quenches the whole magnet coil. Therefore enthalpy limit defines the critical energy and consequently the quench protecting threshold for the BLM system.

The copper specific heat depends on the temperature. The specific heat of Niobium-Titanium alloy depends also on the magnetic field inside the superconductor, therefore it varies in different parts of the coil.

One of the first calculations of the cable enthalpy of LHC dipole [7] reported values of 38 mJ/cm^3 for injection energy and 0.8 mJ/cm^3 for collision energy. Refined calculations [6] which take into account updated value of copper-to-superconductor

[2]There is an evidence that the helium contained in the cable can participate in the strand cooling for times below 100 μs.

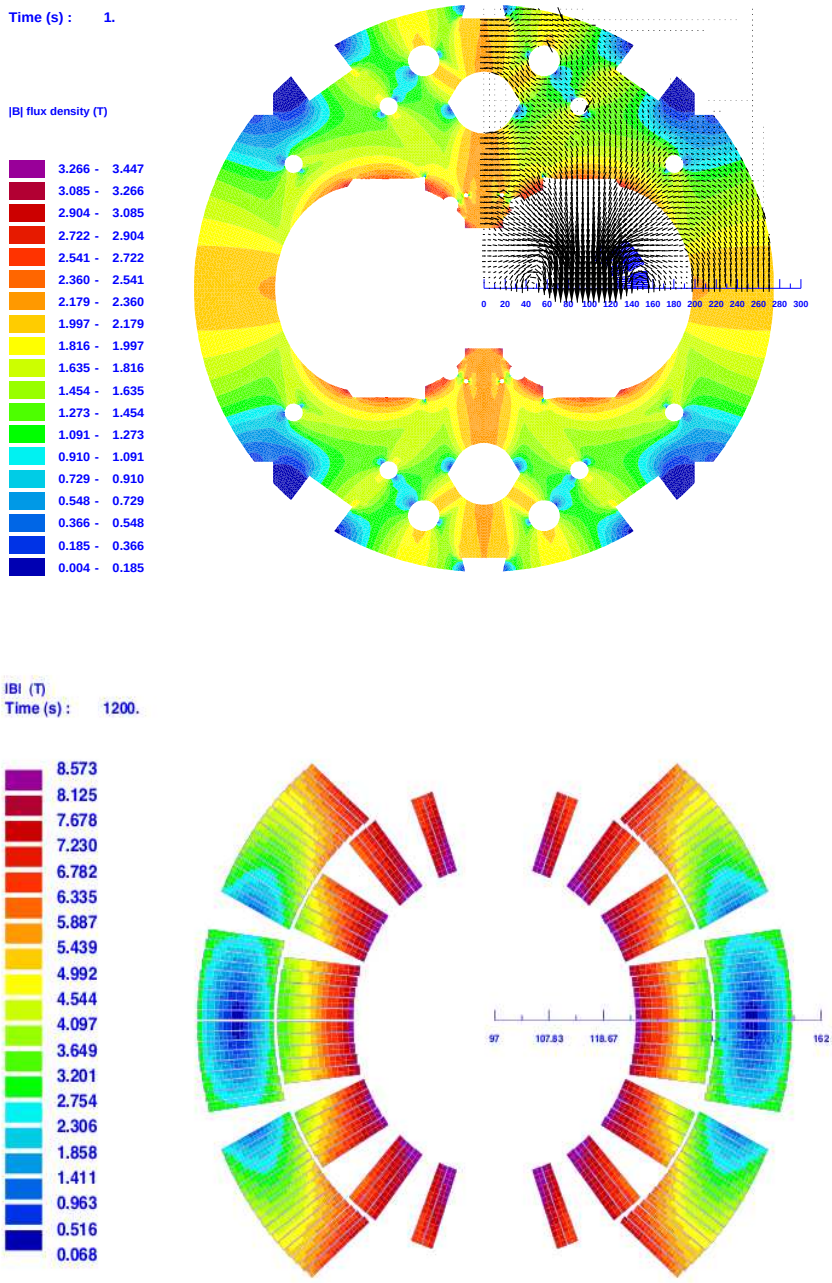

Figure 2: *The magnetic field of the MB magnet at collision energy. Upper plot: the transverse vector field is shown for one quarter of the magnet. The color code shows the field intensity in the iron yoke. In simulation the field is symmetrically cloned to the other 3 quarters of the magnet cross section. Bottom plot: field inside the coil. The field is calculated by ROXIE.*

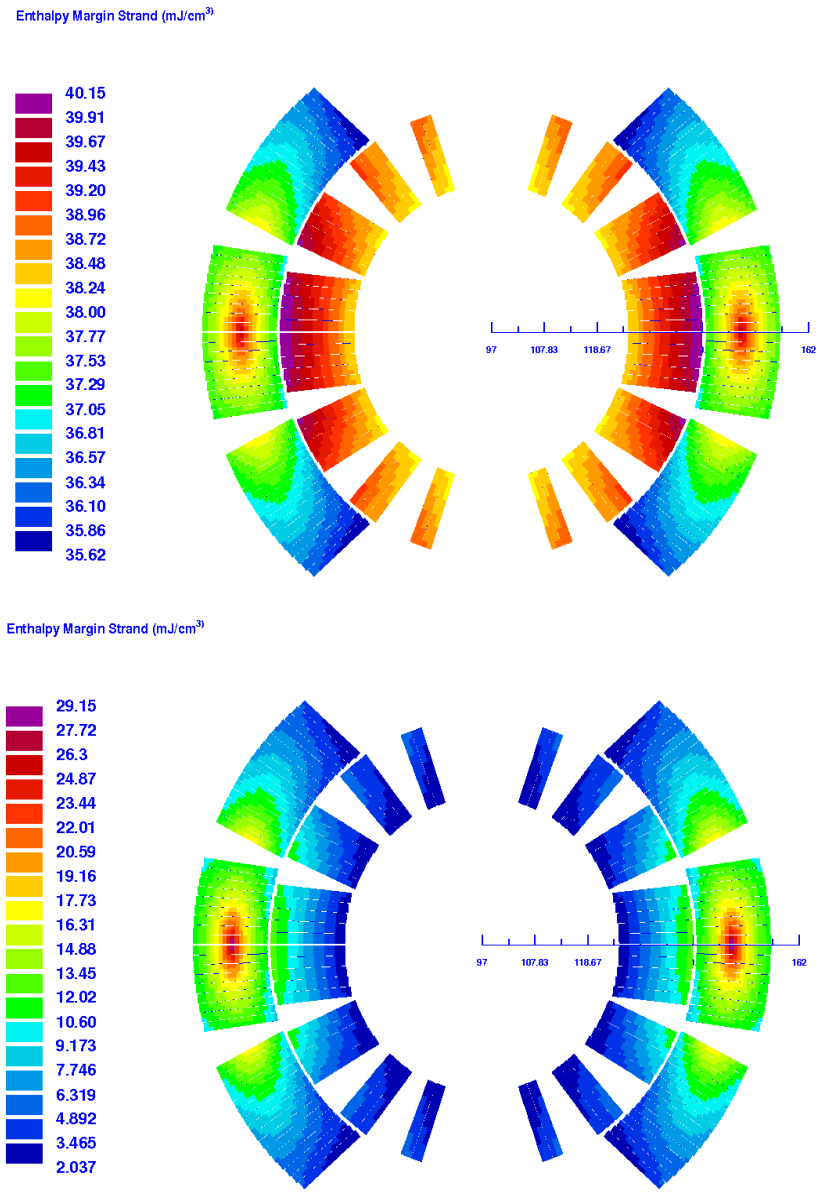

Figure 3: *Distribution of the Quench Margin on the transverse cross section of the coil, for injection (upper plot) and nominal (bottom plot) currents of MB magnet. Courtesy of [18].*

ratio show respectively 31.3 mJ/cm^3 and 0.93 mJ/cm^3 for Type-1 cable (i.e. inner coil). The cable enthalpy limit calculations has been also implemented in ROXIE [17, 18]. An example of the map of enthalpy limit across the coil cross section from ROXIE is presented in Figure 3. The most fragile region is situated in the external cables of the outer coil where the enthalpy density limit $H_{strand} = 35.62$ mJ/cm^3,

and in the part of the coil most exposed to losses it reaches H_{strand} =38.24 mJ/cm^3.

For collision energy the map of the enthalpy limit shows the most fragile region in the place most exposed to energy deposition from beam losses which is the internal surface of the inner coil. The value of the enthalpy density limit is H_{strand} =2.04 mJ/cm^3.

For comparison of the different the enthalpy density limits are shown on the left plot of Figure 8. The results given by ROXIE are larger then the one obtained in [6] by almost 20% for injection energy and factor 2 for collision energy. The discrepancy is caused mainly by different assumptions concerning the magnetic field distribution in the coil, the paramtrizations of the specific heat and the numerical integration methods. In the threshold estimation the most conservative values have been used and they are presented in Table 1.

In case of steady state losses, also discussed in this paper the quench limit is estimated from complex models of heat transport inside the magnets [8, 9]. According to these models, the power which can be evacuated from the magnet coil without quenching the magnet is between about 320 mW/cm^3 for injection and 12 mW/cm^3 for collision energies, but these values depend on the heat density distribution in the coil.

5 Distributed losses

For practical reasons the distributed losses are obtained by convoluting pointlike losses with a broad gauss distribution. The width of this distribution is given by the beam intensity distribution and the impacting angle. Typically it is larger than the coil energy deposition distribution for a single proton (width at half height of about 50 cm) as well as the width of the signal outside the cryostat (width at half height of about 200 cm).

In this study a proton impact distribution with $\sigma_{loss} = 4.0$ m is used, the same as the one observed during the first quench event (Section 9). This loss corresponds to a typical situation of LHC beam (with $\sigma_{beam} = 1$ mm) being lost with the impacting angle of 240 μrad.

On the right plot of Figure 1 a loss profile along the beam screen is shown for loss of single 3-dimensional bunch with $\sigma_{beam} = 1$ mm ($\sigma_x = \sigma_y$) and with longitudinal gaussian distribution with $\sigma_{long} = 75.5$ mm impacting with angle 240 μrad. The loss distribution depends on the transverse width of the beam in direction perpendicular to the beam screen (σ_y in case of vertical loss) and on the impact angle. It is independent on transverse profile of the beam in direction paralel to the beam screen surface (σ_x in case of vertical loss) and on longitudinal beam profile. Therefore the loss distribution of a gaussian bunch is a gaussian along the beam screen.

Wider loss distribution leads to higher thresholds and more localized losses correspond to lower threshold (see Section 8). The lowest thresholds are due to pointlike losses which could happen due to presence of an obstacle in the beam aperture. In case of the MB magnet there are no aperture changes along the magnet, therefore

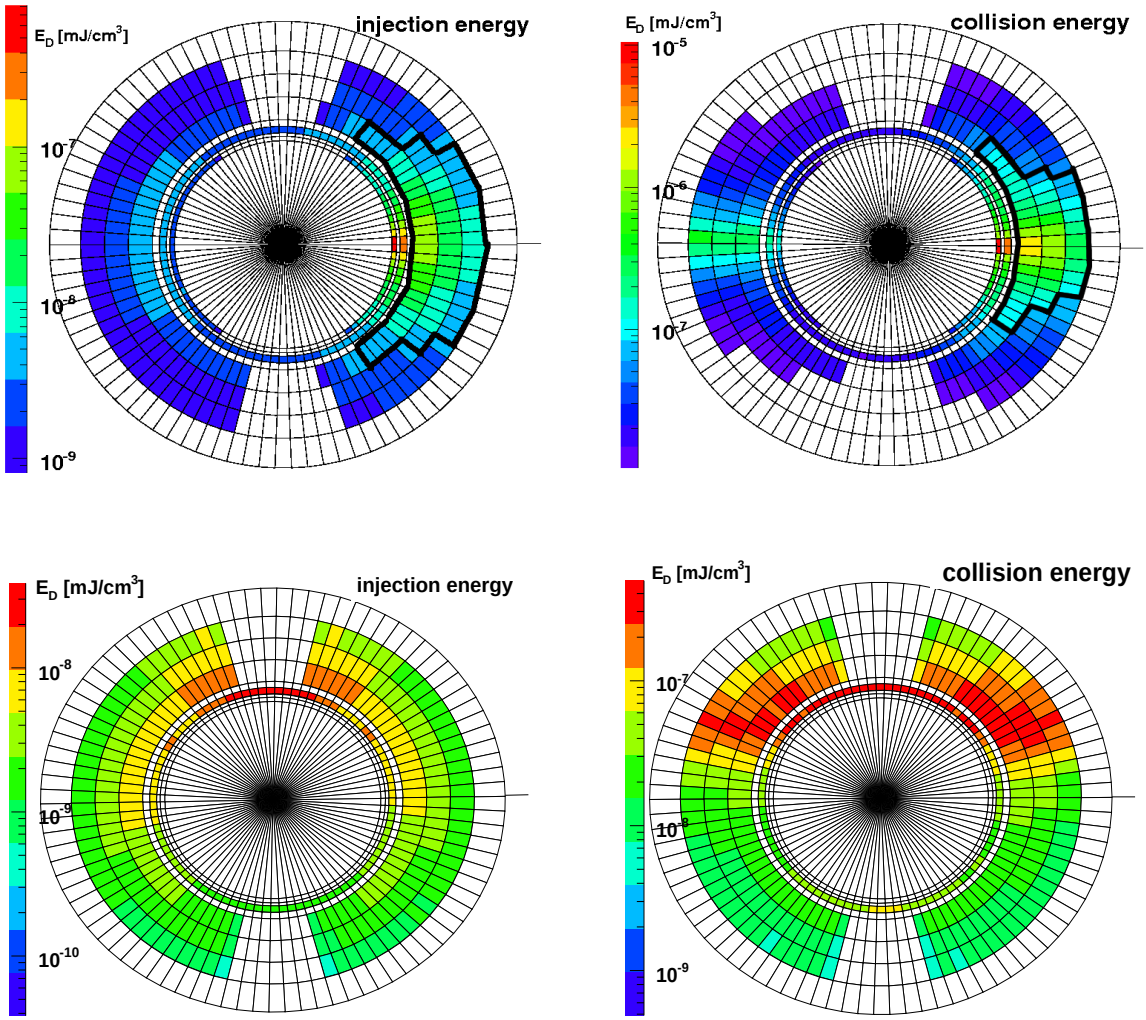

Figure 4: *Cross section through the region of MB internal coil with maximum energy deposition (per proton, for pointlike loss) for injection and collision beam energies. Upper plots show horizontal loss and areas marked contain 90% of the energy deposition in the cross section of the right coil. Down plots show vertical loss and in this case the energy deposition in beam screen is not shown.*

the typical loss distribution, as presented above, has been chosen as the one defining threshold in the Beam Loss Monitors.

6 Energy deposition in the coil

The energy is deposited in the magnet coil by the hadronic cascade which starts to develop in the beam screen. Because of a small impacting angle only a part of the cascade heats the coil. Typically only about 15-20% of the initial proton energy is released in the coil (including the copper wedges). About 5% is released in the beam screen and in the cold bore. The rest is deposited in the collar or yoke or scattered back to the vacuum pipe and might heat up other parts of the magnet or the elements downstream the magnet.

In Figure 4 the energy density (E_D) distribution on the magnet cross section in the most exposed plane is shown. The energy density in the beam screen and in the cold bore are a factor few higher than in the coil. The comparison of situation at injection and collision energies shows that a higher magnetic field leads to lower vertical and higher horizontal spread of the energy, resulting in the energy concentration in the horizontal plane. To quantify this effect a thick line surrounding a region containing 90% of the total energy deposited in the right coil is drawn. In case of injection energy the "90% region" is made of 63 cells which constitute about 55% of the cross section of the coil. In case of collision energy this region shrinks down to only 46 cells i.e. 40% of the coil cross section surface.

In case of vertical losses the magnetic field changes the direction of the cascade so much, that the maximum is about 60 degrees from the initial proton direction. Therefore the fragile external cables of the coil are less affected by the loss. At collision energy there are no vertical losses for the cascade.

In the Figure 5 the energy density for the most exposed azimuth of the coil is shown as a function of longitudinal distance from the loss location for four configurations of the beam energy and the loss location. The red, blue and black points correspond to the three radial layers of bins in which the energy density is determined.

For injection energy the maximum of about $8 \cdot 10^{-8}$ mJ/cm^3 per impacting proton is reached for the innermost part of the coil (red points) at about $l_{peak} = 35$ cm from the loss location. It is interesting to notice that in case of vertical loss the maximum energy is only about 30% of the one seen for horizontal loss. This happens because in case of vertical loss the superconductor more distant from the loss location then in case of vertical loss.

For collision energy the peak position remains the same, but the maximum value raises by a factor of about 31 for horizontal loss and factor 20 for vertical one. The impacting protons energy increases by factor 15, but the magnetic field increases the deposited energy density.

6.1 Energy density as a function of radius

The maximum energy deposition (E_D^{max}) is located on the inner surface of the coil. The value of E_D^{max} is deduced from the radial dependence of E_D for three radial bins

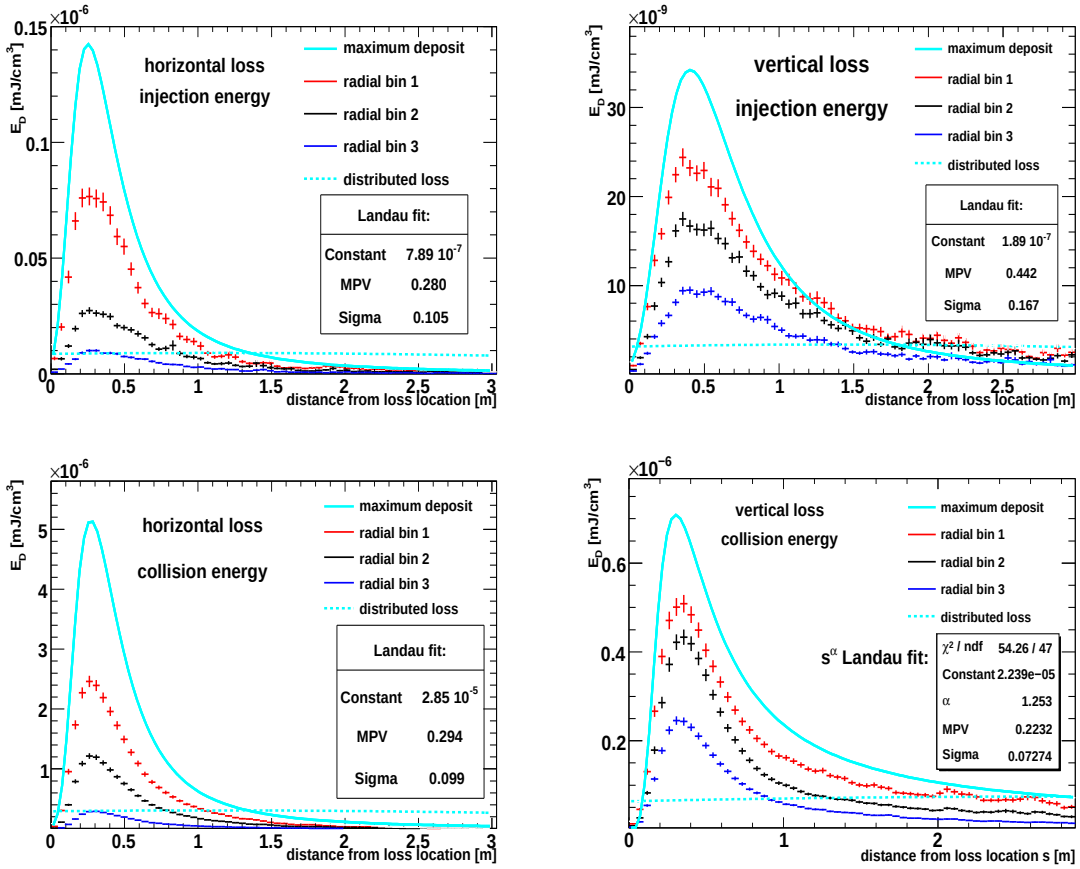

Figure 5: *Energy density distribution per impacting proton for the most exposed azimuth in three layers of coil (red being the innermost one and blue the outermost) as a function of distance from the loss location. Plots are made for two loss locations (horizontal and vertical) and for injection and collision beam energy. The blue continuous line represents the estimation of the maximum energy at the inner surface of the coil. The Landau fit describes this line. The blue dashed line represents the expected energy deposition in case of distributed loss.*

registered in the simulation. The radial dependence is fitted with an exponent or a power law and the value of the function at the coil inner radius is determined. The method is similar to the one used in [7], but for high energies, because of the magnetic field effect, the beam screen and cold bore are excluded from the fit.

The procedure is illustrated in Figure 6, where the maximum energy is plotted for the beam screen, the cold bore and for the three layers in the coil. In case of injection energy the distribution is fitted with the same power-law function as the one used in [7]. The exponent value is found to be $p_2 = 2.40$ while [7] reports value $p_2 = 1.76$.

The right plot of Figure 6 illustrates the effect of the magnetic field on the shape

of the transverse energy distribution at high beam energy. The distribution is shown with (red) and without (black) magnetic field. The distribution with the magnetic field does not follow the power law in the whole range of radius anymore. Because of the magnetic field the concentration of energy in the coil is observed, while the energy deposition in the beam screen and in the cold bore is lower then in the case without the magnetic field. The radial distribution inside the coil is well described by a simple power law function with exponent $p_2 = 1$, and this fit is later used to determine the energy deposition on the internal surface of the coil (E_D^{max}). The distribution without magnetic field can be fitted with a power law for all layers, including cold bore and beam screen. In this case the exponent is about 3.25, while the study [7] reports value of 1.15.

To quantify the magnetic field effect a 90% cluster, as in the Figure 4, is used. Without the magnetic field the 90% of the energy is deposited in 68 bins [3], and with magnetic field this number goes down to 46.

The estimation of the maximum energy density is an important part of the threshold determination procedure. It is made by fitting the radial energy distribution and finding the fit value for the location of the inner surface of the coil.

The ratio between the maximum energy density estimated from fit (E_D^{max}) and the energy density in the most inner layer (E_D^{in}) has the following properties:

- for injection energy and horizontal loss $E_D^{max}/E_D^{in} = 1.8$ in the peak (l_{peak}) and 1.4 ($l_{tail} = 2$ m) the tail of the cascade,
- for injection energy and vertical loss $E_D^{max}/E_D^{in} = 1.3$ in the peak and 1.1 the tail of the cascade,
- for collision energy and horizontal loss $E_D^{max}/E_D^{in} = 2.3$ in the peak and 1.5 the tail of the cascade,
- for collision energy and vertical loss $E_D^{max}/E_D^{in} = 1.4$ in the peak and 1.2 the tail of the cascade.

The effect of the cascade compactification due to magnetic field is visible in the fact that the ratio in the most inner layer of the coil E_D^{max}/E_D^{in} increases with the beam energy.

In the following analysis the maximum energy deposition in the coil is used. The error of estimation of the E_D^{max} depends on the beam energy. For injection energy the radial energy distribution is well fitted with the power law and the error, estimated from errors of fit parameters, is about 10%. For collision energy the distribution is distorted and cannot be fitted with a physical dependency in the whole range. Therefore the fit is restricted to the coil. The error of E_D^{max} determination is about

[3] In case of loss at injection energy this number is 64 cells, which is less then without magnetic field, so some effect of the magnetic field on the maximum energy density of the cascade is visible already at injection.

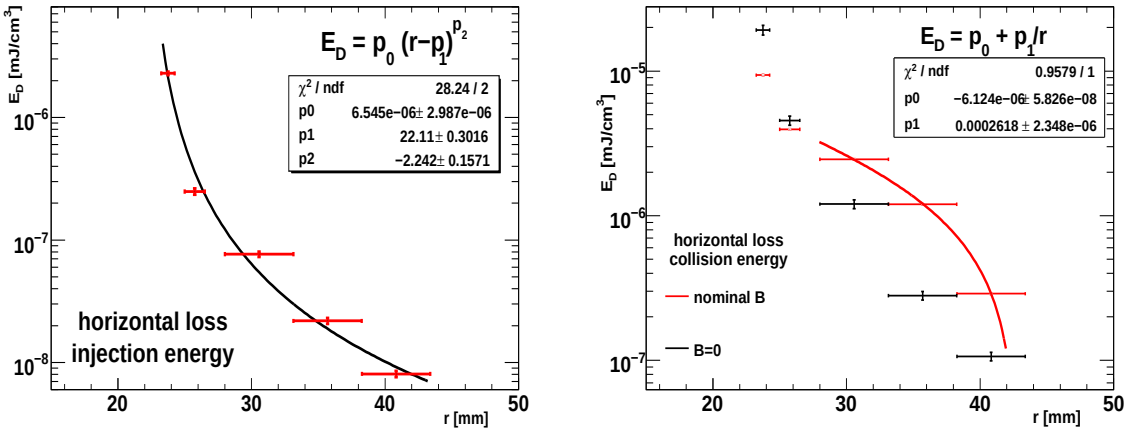

Figure 6: *Maximum energy density along the most exposed azimuth. Left plot is for injection energy and horizontal loss and the right one is for collision energy. For collision energy the radial dependence of* E_D *does not follow a single power law in the whole range of radius. It is fitted with a simple power law with exponent one inside the coil excluding the values in the beam screen and the cold bore.*

20%. For both beam energies a 5% statistical error due to the finite Monte Carlo sample is added.

6.2 Maximum energy density as a function of beam energy

The maximum energy deposition in the cascade increases with the impacting proton energy (E_{beam}). The parametrizations of hadronic cascade profile found in the literature do not apply directly to the geometry of the magnet, where the impacting angle is very small and the beam screen together with the cold bore protect the magnet coil.

In the previous studies [19] the Parametrization 1 has been used.

$$E_D^{max} = C_1 \cdot E_{beam} \cdot \log(5.2\ E_{beam}) \tag{1}$$

Here it is found that the power law with exponent of 1.53 fits better the results of the simulation [4]. In case of distributed loss a good fit has been found to be $E_D^{max}[mJ/cm^3] = 7.21 \cdot 10^{-9} E_{beam}^{1.25}$ [TeV], so with smaller exponent then in case of the pointlike losses. The power law fit to the maximum energy density deposition as a function of the beam energy for horizontal loss is presented in Figure 7.

In the Tables 1 and 2 the maximum energy deposition in the coil (E_D^{max}) as a function of beam energy is presented, together with the enthalpy limit of the cable (H_{cable}) and the BLM signal (Q_{BLM}) for the detector placed in the optimal location

[4] TableCurve2D program was used to test which dependency fits best the results of the Monte Carlo simulation.

beam energy [TeV]	E_D^{max} [mJ/cm^3] per proton	enthalpy limit H_{strand} [mJ/cm^3]	protons to quench	BLM signal Q_{BLM} [aC/prot]
horizontal, pointlike loss				
0.45	$1.45 \cdot 10^{-7}$	31.29	$2.16 \cdot 10^{8}$	33.8
1	$3.27 \cdot 10^{-7}$	24.60	$7.52 \cdot 10^{7}$	67.2
2	$8.10 \cdot 10^{-7}$	15.26	$1.88 \cdot 10^{7}$	137.8
3	$1.39 \cdot 10^{-6}$	8.90	$6.38 \cdot 10^{6}$	235.2
4	$2.64 \cdot 10^{-6}$	4.83	$1.83 \cdot 10^{6}$	344.1
5	$3.95 \cdot 10^{-6}$	2.46	$6.22 \cdot 10^{5}$	596.3
6	$5.03 \cdot 10^{-6}$	1.29	$2.57 \cdot 10^{5}$	657.3
7	$5.59 \cdot 10^{-6}$	0.93	$1.66 \cdot 10^{5}$	788.6
vertical, pointlike loss				
0.45	$2.68 \cdot 10^{-8}$	31.29	$1.17 \cdot 10^{9}$	19.8
7	$7.12 \cdot 10^{-7}$	0.93	$1.31 \cdot 10^{6}$	828.7

Table 1: *Maximal energy density depositions* E_D^{max} *(per proton), cable enthalpy margin (*H_{strand} *), the number of protons to quench the magnet (*N_p^{QL}*) and the signal in the BLM in maximum (*Q_{BLM}*). The values are presented for* **pointlike losses***, in case of various beam energies and for horizontal and vertical loss locations.*

(in the signal maximum). The method used to obtain BLM signal is described in Section 7.4. The Table 1 is made for pointlike losses while the Table 2 the same is presented for distributed losses.

The Figure 5 shows longitudinal profile of E_D for different radial bins (depths) of the coil. The blue line shows the maximum value expected on the inner surface of the coil. The distributions are fitted with Landau curve. The typical width of the cascade in the coil, in terms of σ_{landau}, is about 10 to 15 cm, and the Full Width at Half Maximum (FWHM) is about 50 cm.

For injection energy the amount of protons necessary to be lost in a single location to quench the magnet is about $N_p^{QL} = 2.16 \cdot 10^8$. If the vertical loss is considered the energy deposit in the coil is smaller and $1.17 \cdot 10^9$ (5 times more) protons are necessary to be lost in a single location to quench the magnet. For collision energy the corresponding numbers are: $1.66 \cdot 10^5$ and $1.31 \cdot 10^6$ protons (8 times more). Therefore at the collision energy the difference between vertical and horizontal loss is larger then for injection energy. This can be explained by the effect of energy concentration due to magnetic field which is more important for horizontal loss then for the vertical one.

In case of distributed losses (Table 2) the reduction of the maximum energy density to the level of 10-16% of E_D^{max} is expected. The critical conditions are expressed in protons lost per one meter of the vacuum pipe. This value is read from the peak of the loss distribution as the one presented on the right plot of Figure 1. The maximum vary from $4.07 \cdot 10^8$ p/m to $6.95 \cdot 10^5$ p/m for horizontal loss. Therefore

beam energy [TeV]	E_D^{max} [mJ/cm^3] per proton	enthalpy limit H_{strand} [mJ/cm^3]	protons/m to quench	BLM signal Q_{BLM} [aC/prot]
horizontal, distributed loss				
0.45	$7.28 \cdot 10^{-9}$	31.29	$4.07 \cdot 10^{8}$	6.2
1	$1.85 \cdot 10^{-8}$	24.60	$1.26 \cdot 10^{8}$	13.6
2	$3.52 \cdot 10^{-8}$	15.26	$4.10 \cdot 10^{7}$	26.2
3	$5.97 \cdot 10^{-8}$	8.90	$1.41 \cdot 10^{7}$	43.5
4	$6.50 \cdot 10^{-8}$	4.83	$7.05 \cdot 10^{6}$	61.9
5	$8.64 \cdot 10^{-8}$	2.46	$2.69 \cdot 10^{6}$	109.5
6	$1.12 \cdot 10^{-7}$	1.29	$1.09 \cdot 10^{6}$	126.2
7	$1.27 \cdot 10^{-7}$	0.93	$6.95 \cdot 10^{5}$	145.5
vertical, distributed loss				
0.45	$2.10 \cdot 10^{-9}$	31.29	$1.41 \cdot 10^{9}$	5.1
7	$3.58 \cdot 10^{-8}$	0.93	$2.55 \cdot 10^{6}$	189.9

Table 2: *Maximal energy density depositions* E_D *(per proton), quench margin in the cable and signal in the BLM (per proton) from the loss location for different beam energies and for horizontal and vertical losses. Values for* **distributed losses**.

the amount of protons lost per meter to quench the magnet is about 2 times more then in the case of pointlike losses [5].

The ratio of the BLM signal to the maximum energy deposit in the coil is about 5 times higher for the distributed losses than for the pointlike ones because the width of the energy distribution in the coil is about 5 times smaller then the width of the signal outside the cryostat.

6.3 Energy density in thermal equilibrium volume

In order to draw preliminary conclusions about thresholds in case of steady state beam losses a maximum energy deposition in thermal equilibrium volume should be considered. The thermal equilibrium volume is a cable volume in which the heat deposited by the beam has time to dissipate. This volume in case of superconducting coil correspond to a piece of cable with length corresponding to the transposition pitch of the cable which, in case of inner layer of MB coil, is 11.5 cm. Energy density measured in this volume is called E_D^{cable} .

In this study, due to technical reasons, the angular size of cell in which E_D^{cable} is measured correspond to two cables (4 °). This leads to underestimation of E_D^{cable} by less then 10%. The volume of thermal equlibriul is 1.682 cm^3. For comparison the volumes used in study [20] are between 1.551 cm^3 and 2.754 cm^3.

[5] One should keep in mind that quantities of different dimensions are compared here, it is done in order to confront these numbers with [7]

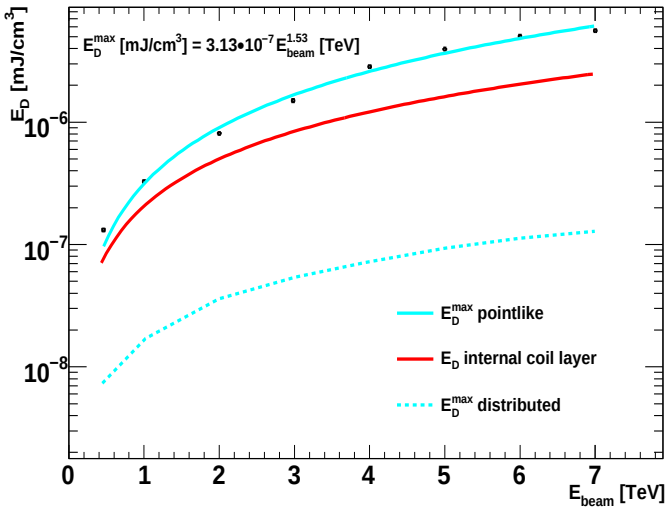

Figure 7: *The plot shows the evolution of the energy deposition in the coil with the impacting proton energy. The red curve presents the evolution in the most inner bin of the coil, the blue shows the extrapolated maximum energy deposition which takes place at the inner surface of the coil and the dashed line shows the deposition for the distributed losses.*

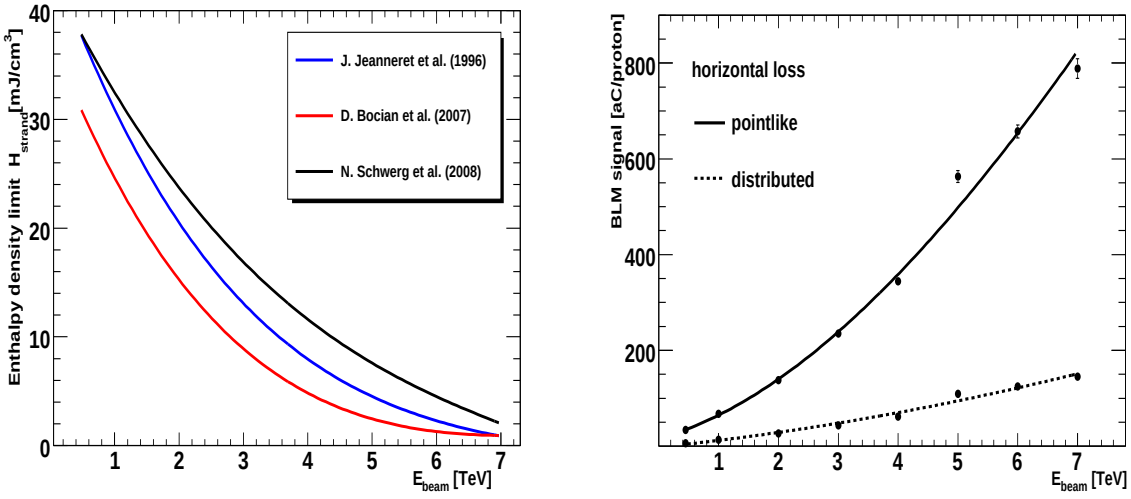

Figure 8: *Illustration of the results from Table 1. Left plot: Cable enthalpy as a function of beam energy. Results of various studies are presented. Right plot: Signal in the BLM, per interacting proton, in the maximum (solid line) as a function of beam energy. Dashed line shows the signal level for distributed loss.*

In Table 3 the values of E_D^{cable} and the quench limits are shown. From comparison with Tables 1 and 2 it can be concluded that E_D^{cable} is about 5 times smaller then

E_{beam} [TeV]	E_D^{cable} [mJ/cm^3] per proton	quench limit P_{QL}[mW/cm^3]	proton rate to quench [s^{-1}]	proton rate in max [s^{-1}m^{-1}]
horizontal, pointlike loss				
0.45	$2.43 \cdot 10^{-8}$	320	$1.32 \cdot 10^{10}$	-
7	$8.05 \cdot 10^{-7}$	12	$1.49 \cdot 10^{7}$	-
vertical, pointlike loss				
0.45	$1.08 \cdot 10^{-8}$	320	$2.96 \cdot 10^{10}$	-
7	$4.21 \cdot 10^{-7}$	12	$2.85 \cdot 10^{7}$	-
horizontal, distributed loss				
0.45	$1.22 \cdot 10^{-9}$	320	$2.63 \cdot 10^{11}$	$2.58 \cdot 10^{10}$
7	$1.83 \cdot 10^{-8}$	12	$6.56 \cdot 10^{8}$	$6.45 \cdot 10^{7}$
vertical, distributed loss				
0.45	$8.50 \cdot 10^{-10}$	320	$3.77 \cdot 10^{11}$	$3.71 \cdot 10^{10}$
7	$6.22 \cdot 10^{-9}$	12	$1.92 \cdot 10^{9}$	$1.89 \cdot 10^{8}$

Table 3: *Energy density depositions in thermal equloibrium volumes* E_D^{cable} *(per proton), quench margin in the cable and the resulting maximal proton loss rate for various loss configurations and beam energies. In case of distributed loss a loss rate density in the loss maximum is also given.*

E_D^{max} in case of horizontal losses. In case of vertical losses the difference is smaller.

In Figure 9 a longitudinal profile of E_D^{cable} is shown. The profile shape is almost identical with the profile for E_D^{max} , therefore the smearing procedure leads to a very similar decrease of energy deposition in the maximum of the cascade.

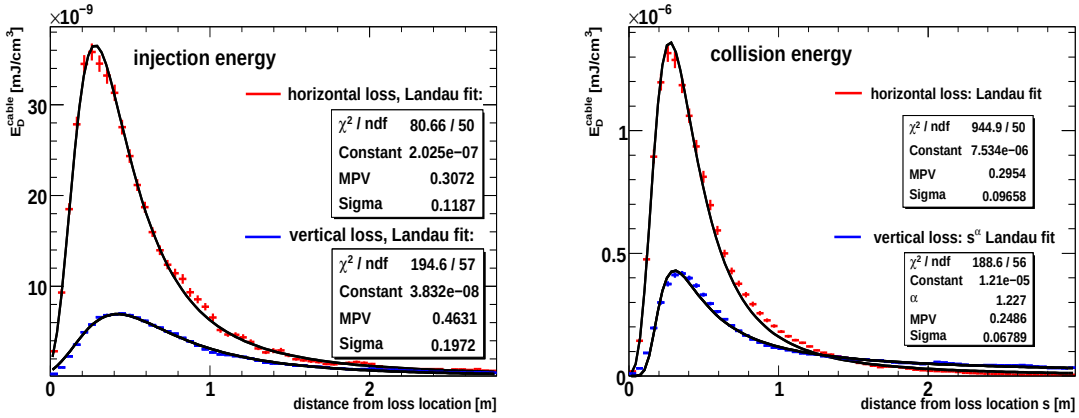

Figure 9: *Energy density distribution per impacting proton for the most exposed azimuth in the thermal equlibrium volume of the inner coil. The shape of the distribution is the same as in case of* E_D^{max} .

7 Signals in Beam Loss Monitors

In this Section the particle fluence outside the magnet cryostat and the resulting signals in the Beam Loss Monitors are discussed. The angular distribution of particles hitting the BLMs is shown and the method to calculated signal using response functions is presented.

7.1 Multiplicity of particles outside cryostat

For comparison with previous studies [12] a distribution of multiplicity of particles outside the cryostat in the placement of left and right BLMs is shown in Figure 10 and 11. The red histograms correspond to the particles hitting the BLM originating from beam 1 and the blue ones to BLM on opposite beam. The presence of the signal in the BLM surveying the opposite beam is called cross-talk [21]. Here we define it as a ratio of the fluence of particles arriving to the BLM on the opposite beam to the fluence of particles arriving to the BLM which is desingted to measure the beam.

For horizontal loss the cross-talk is about 0.22 at injection energy (left plot of Figure 10) and 0.30 for collision energy (left plot of Figure 11). For the vertical loss, (right plot of Figure 10 and of Figure 11) the cross-talk is 0.30 at injection energy and 0.15 at collision energy. In all cases the maximum of the fluence distribution is at a distance of about 1 meter from the loss location.

It is unexpected that cross-talk for vertical loss is smaller then for the horizontal one.

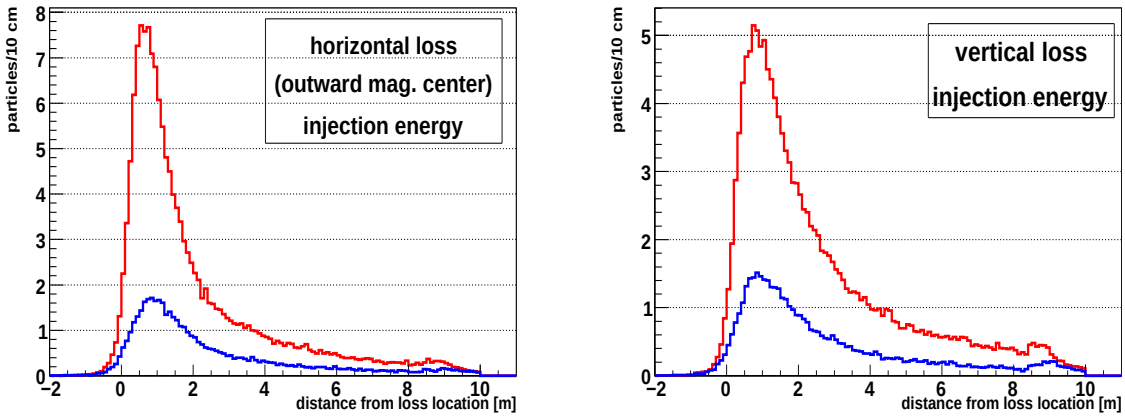

Figure 10: *Multiplicity of particles outside cryostat in the direction of the beam loss (red histogram) and in the opposite direction (sometimes refereed as a "cross-talk signal", blue histogram). Left plot: injection beam, vertical loss, right plot: injection beam, horizontal loss (outward magnet center).*

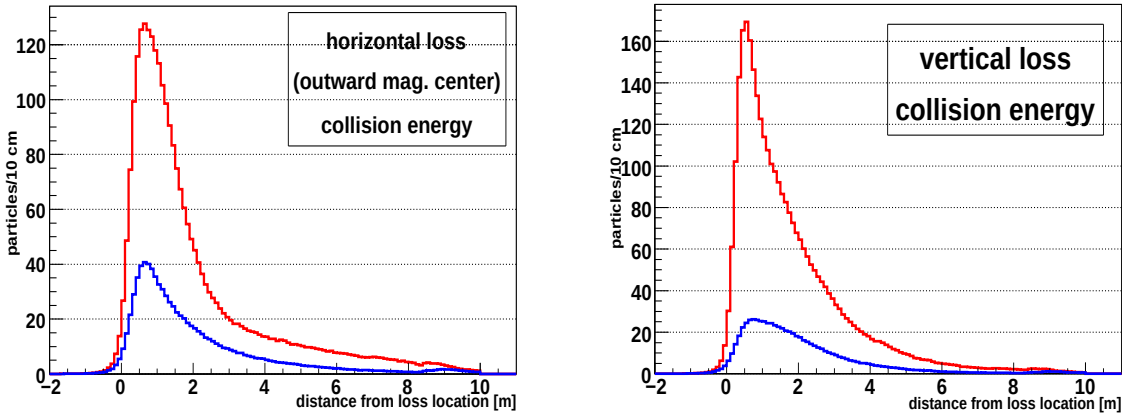

Figure 11: *Left plot: Multiplicity of particles outside cryostat in the direction of the beam loss (red histogram) and in the opposite direction BLMs (sometimes refereed as a "cross-talk signal", blue histogram). Collision beam, horizontal loss (outward magnet center). Right plot: the same for vertical loss.*

7.2 Spectra and angular distribution

The particles leaving the cryostat and entering the BLMs are mostly perpendicular to the BLM axis. The typical angular distribution is shown in Figure 12. The entry angle is defined as an angle between BLM longitudinal axis and the particle momentum vector. As it can be seen on the left plot of Figure 12 most of the particles enter the detector almost perpendicularly to the BLM longitudinal axis.

The distribution is not forward-backward symmetric: there are more particles entering the chamber from the direction of the beam. The chambers are not symmetric - there is an electronic compartment on one side. It has been shown in CERF experiment [22] that the impact of the electronic compartment on the total signal registered by the chamber is small. Therefore here the chambers are treated as symmetric cyllinders.

In the Figure 13 the spectra of particles hitting the BLM 75 cm after the loss location are presented. The two dominant components are neutrons and gammas. For both: collision and interaction energies the maximum of the spectrum is at about 0.3 MeV. The most energetic components of the spectra are protons and pions.

The differential spectra, presented in the bottom row of Figure 13, show that the spectra of most types of particles follow in a part of the energy range a baseline power law with exponent of about -0.6. The dominantion of neutrons and photos is even more visible on these plots. These particles almost never follow the power law.

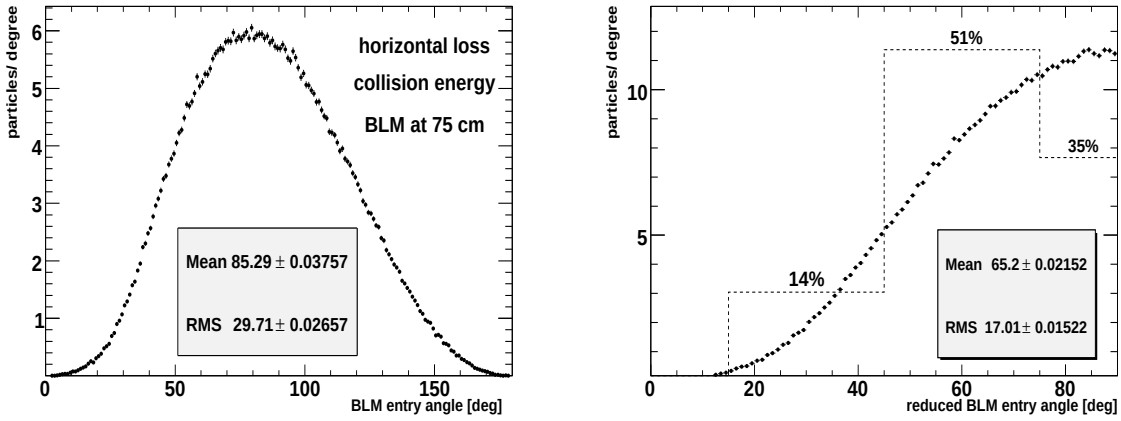

Figure 12: *Left plot: angular distributions of particles entering BLM at 75 cm from the loss location. Right plot: Angular distribution of particles hitting the BLM, collision energy, horizontal loss. The dashed lines show the fractions of the fluence convoluted with the four response functions (see Section 7.4).*

7.3 Response functions

Response functions give a charge generated by a passage of a single particle through the Ionisation Chamber. The response depends on particle energy and on the impact angle. The response functions have been produced used the simulation code from [15], but using a different procedure.

The energy range considered in response function production is between 900 eV and 1 TeV. Due to limited computing power the whole range has been divided into 90 bins. In case of neutrons the considered energy range has been extended down to almost 10^{-4} eV in order to generate response to the thermal part of the spectrum. In this case the response function determination has been performed in 150 bins.

For every bin a flat spectrum of impacting particles has been generated. The simulation has been performed for a few selected impact angles. Every time the particles were generated on the surface which corresponds to projection of the chamber shape at the given angle.

The response at small angles, where the particles has to pass more of the chamber material, give higher signal. It is illustrated on Figure 15, where the same mixed spectra is injected to the chamber at different angles. The response to particles hitting the chamber along its axis is 2.5 times larger than to the particles entering from the side.

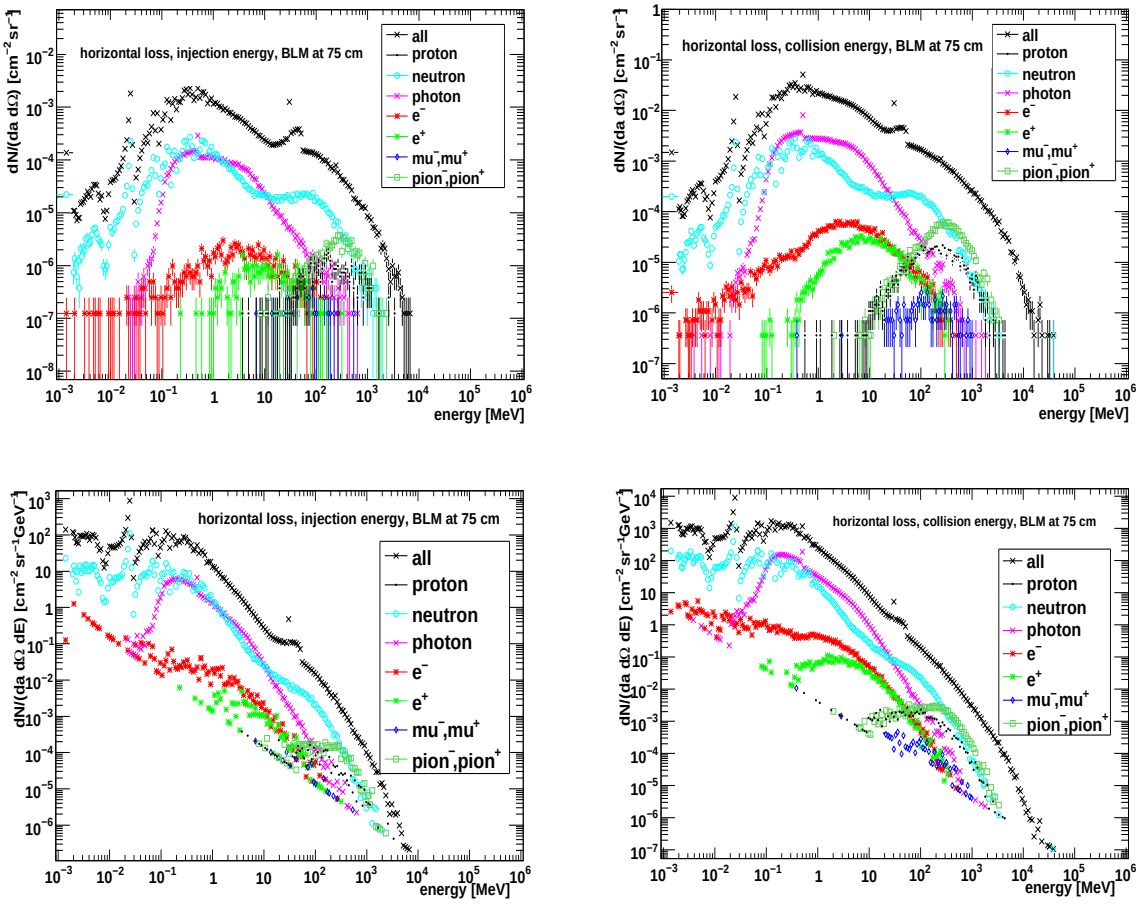

Figure 13: *Upper row: fluence of particles* $\mathrm{dN}/(\mathrm{da}\cdot\mathrm{d}\Omega)$ *per primary proton entering the BLM at beam 1 at 75 cm. Left plot: injection energy, horizontal loss (outward). Right plot: collision energy. Bottom row: the same shown in differential fluence.*

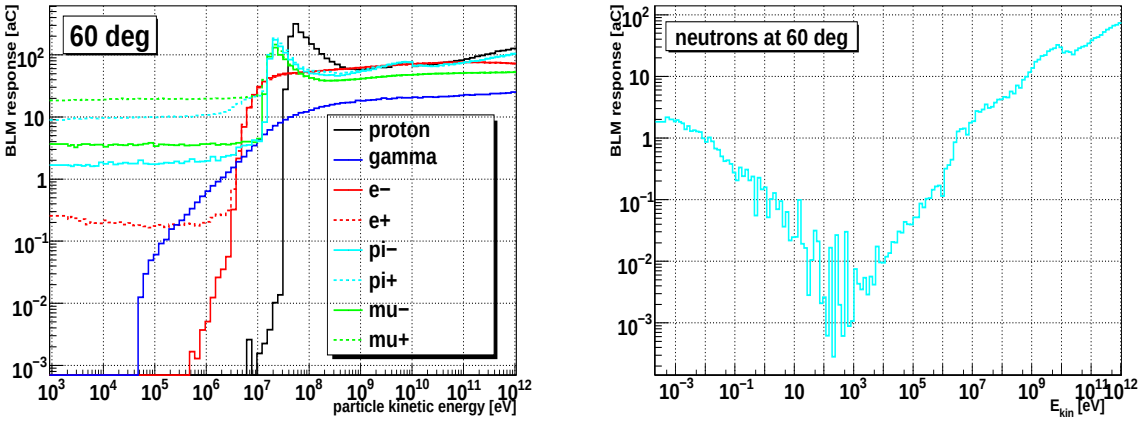

Figure 14: *Response functions for 60˚impact angle. Left plot is for all considered particle types except neutrons, and the right one is for neutrons only.*

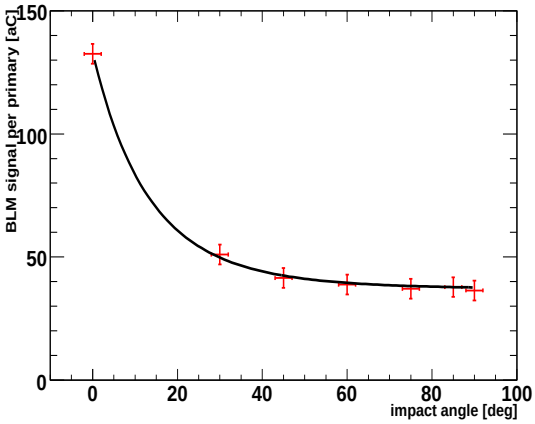

Figure 15: *Response for a typical spectra of particles outside the vacuum tank injected at various angles. The largest response is observed for particles hitting the chamber with small impact angle (along the chamber axis).*

7.4 Signals in Beam Loss Monitors

The signals in the BLMs are calculated by folding the BLM response functions presented in Figure 14 with the spectrum of the particles entering the BLM. An example of such a spectrum is presented in Figure 13. The folding procedure results in signal expressed in charge collected from the BLM electrodes. The procedure is described in [15] and can be described by Equation 2.

$$Q = \sum_{i=1..4} \left(w_i \cdot \sum_{j=p,n,e^-,\gamma...} \sum_{k} R_{i,j,k} N_{j,k} \right) \tag{2}$$

In that Equation the first sum is over the 4 response functions used in this analysis: for 0°, 30°, 60° and 90°([6]). The fluence of particles is folded with the response functions and added with weights (w_i) corresponding to population of particles in the angular bins. The bins are presented as a dashed line on the right plot of Figure 12. The last sum is over binning of the fluence and response function histograms.

The response functions are prepared for the active volume of the detector so they do not include the geometrical inefficiency due to the fact that the particles passing by electronics compartment do not leave a direct signal. This is an approximation because the electronic compartment contains material where particles can interact and the results of the interaction can still reach the active volume and give a signal. But for the typical case of the particles entering the BLM from direction perpendicular to the BLM axis this effect should be very small.

The active volume is 38 cm long, therefore the signal obtained by convoluting spectrum registered outside the cryostat in the 50-cm long slices is multiplied by a factor 0.76.

The additional source of error is the fact that the endings of the BLMs are not simulated (a long tube along the cryostat is simulated) therefore the particles which normally would enter into the sensitive volume through the endings are attributed to a neighbouring BLM. This effect is estimated to be small and BLM acceptance is not corrected for it.

In Figure 16 a process of signal calculation is illustrated in details. On the left-side plots the contributions to the signal from every energy bin and particle type is shown. Right plots show signal integration. The strong neutron fluence, even in energy range between 20 and 200 MeV where neutron component dominates, has relatively small contribution to the total signal. Instead the pions and proton contributions dominate the signal because of the proton and pion peak in the reposnse functions in this energy range. Nevertheless this energy range is particularly important for the neutron contribution and an error made here can strongly affect the total signal.

In the Figure 17 the signals which would appear in BLMs along the cryostat are presented for horizontal and vertical loss and for injection and collision beam energy. The red curve corresponds to the BLM watching the lost beam while the blue one

[6]Functions for 0°and 90°has been obtained with a small tilt, in order to avoid simulation artefacts.

to the BLM on the opposite side of the Cryostat. The dashed line represents signal in case of distributed loss.

The signal is expressed in total dose [Grays]. The pointlike losses are fitted with Landau curves. The maximum of the signal is placed about 1 meter after the loss location. The width of the signal (FWHM) is about 2.5 meters, what is between 4 and 5 times more then the width of the energy density distribution in the coil (see Section 6.2).

This leads afterwords to higher threshold in case of distributed losses then in case of concentrated ones.

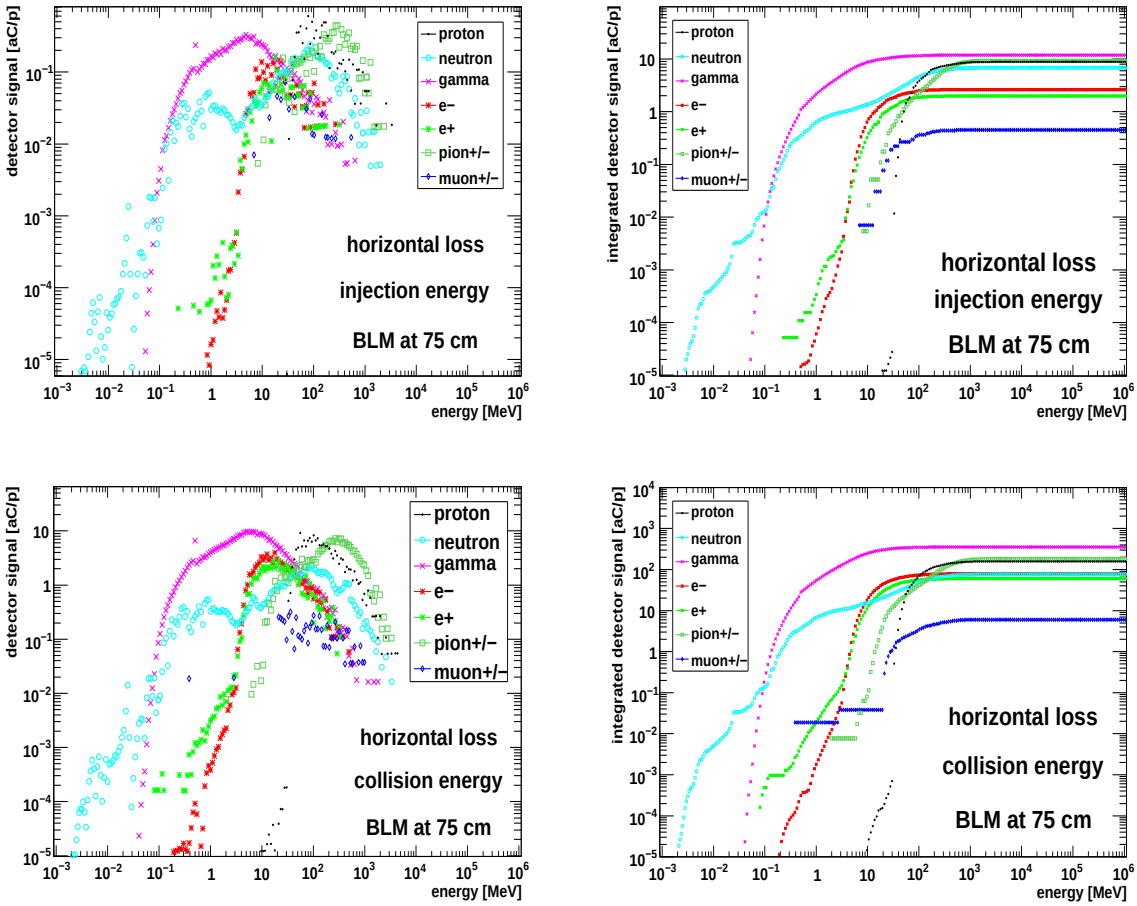

Figure 16: *Contribution (per proton) to the signal in the BLM at 75 cm from 60˚response function as a function of particle type and kinetic energy. Right plots show integrated distributions. Upper row is for loss of injection beam, bottom is at collision energy.*

The contributions of different particle types to the total signal observed by the BLM outside the cryostat are shown in Figure 18. The dominant contribution is

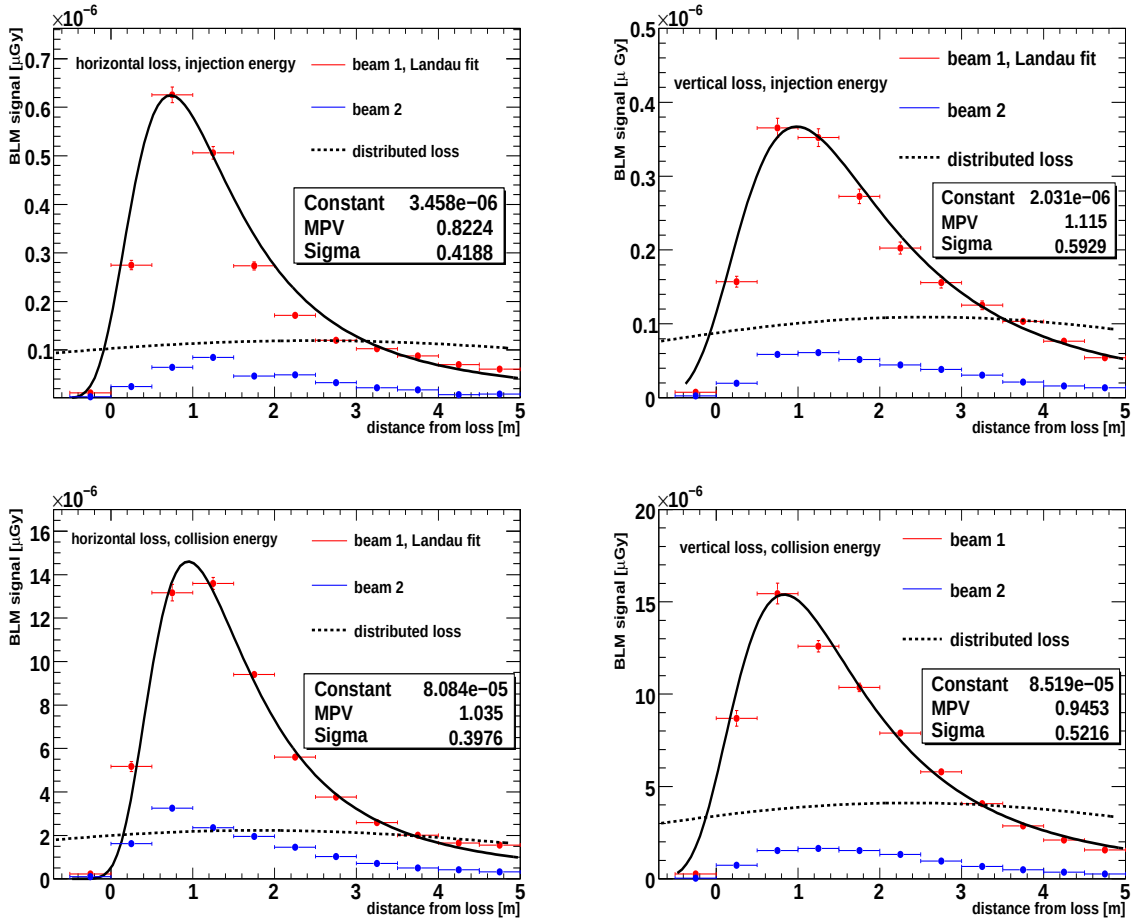

Figure 17: *Signal per impacting proton in BLM cylinders along the cryostat as a function of distance from the loss location. Left upper plot: injection beam, horizontal loss (outwards the magnet center). Right upper plot: injection beam,vertical loss . Row below: for collision energy.*

given by photons, pions and protons. Neutrons give important contribution in case of injection energy and close to the loss location.

The dependence of the BLM signal from the beam energy is shown on the right plot of Figure 8. For distributed loss the dependence can be fitted with a polynomial presented in Formula 3.

$$\mathrm{Q_{BLM}} = -2.12 + 12.9 \cdot \mathrm{E_{beam}} + 1.29 \cdot \mathrm{E^2_{beam}} \tag{3}$$

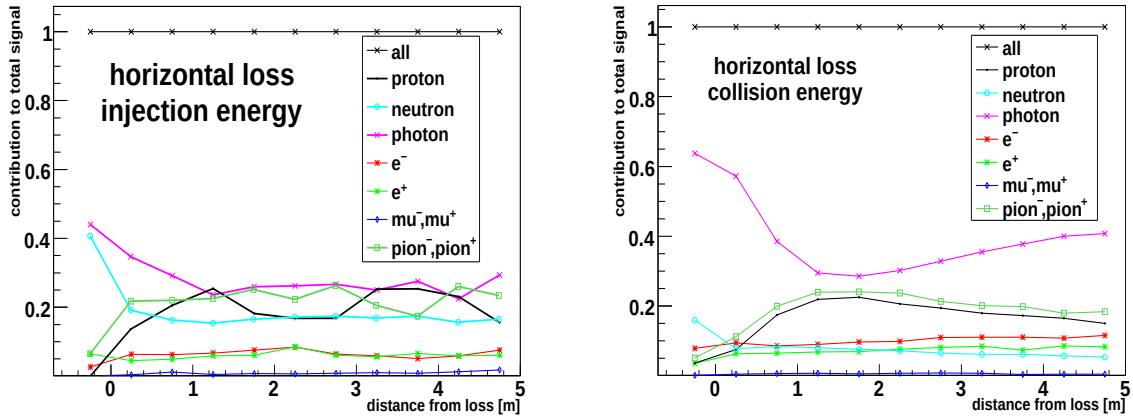

Figure 18: *The contribution of different particle types to the total signal as a function of distance from the loss location.*

8 Quench-protecting thresholds

The quench-protecting threshold (D) is the signal measured by the beam loss monitors corresponding to the energy deposition in the coil equal to the enthalpy limit of the superconducting cable. Reaching the enthalpy limit is not equivalent to a quench of the whole coil, but in order to assure safety of the machine this conservative limit is used. The threshold depends on the beam energy, on the loss type (pointlike or distributed) and on the location of the monitor with respect to the loss (magnet type, monitor position). It depends also on the loss duration but in this report the quench levels are estimated for fast transient losses and for Steady-State ones.

In the Figure 20 the two critical parameters are presented in function of the distance from the loss location: the energy deposit in the coil (E_D^{max}) and the signal in the BLM outside the cryostat (Q_{BLM}). They are presented for pointlike losses. For distributed losses both quantities are spread with gaussian loss distribution. It results in evolution of the threshold value with loss scale as presented on the left plot of Figure 20.

In Table 4 the threshold values are shown for various distances of the BLM from the loss location. They are calculated using Equation 4, where $C_{Gy}^{C} = 5.4 \cdot 10^{-5}$ C/Gy is a conversion factor from Grays to charge deposited in the BLM.

$$D[Gy] = (C_{Gy}^{C})^{-1} \left[Q_{BLM} \cdot H_{cable} \cdot \frac{1}{E_D^{max}} \right] \tag{4}$$

On the right plot of Figure 20 an evolution of the threshold with beam energy is presented. In order to be conservative the lowest thresholds from Table 4 should be set in Beam Loss Monitors. They correspond to horizontal loss in the direction

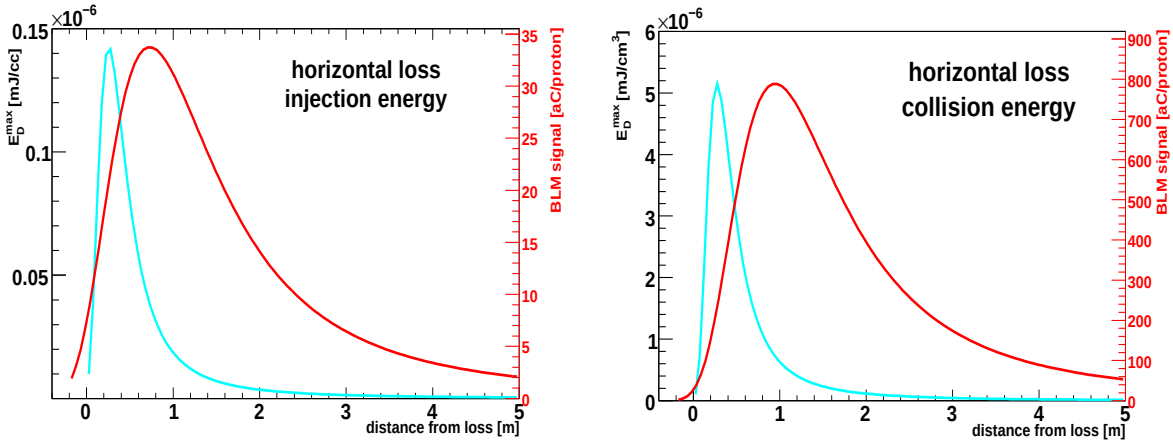

Figure 19: *Illustration of the energy deposition inside the coil and BLM signal outside the cryostat.*

of the magnet center. They change from D_{dist} = 395 μGy for injection energy to D_{dist} = 6.9 μGy at collision. It is worth noticing that difference in the signal from various loss locations at collision energy is larger then at injection energy. This is probably due to the effect of the cascade compression in strong magnetc field as discusses in Section 6.

From Figure 17 it can be concluded that in extreme case of pointlike losses the detectors should be placed every 2-3 meters with thresholds lowered to about 10% of the nominal D_{dist}. In case of distributed losses the minimal distance between BLMs raises and the threshold reaches the asymptotic value for losses distributed over more then 3 meters. But considering a loss of a 7 TeV beam which might be as small as σ_{beam} = 0.2 mm the threshold should be of about 50% of D_{dist} with the distance between BLMs of about 3-4 meters.

8.1 Steady-State thresholds

The steady state thresholds are calculated from Equation 5. The BLM signal (Q_{BLM}) per lost proton is the same as for transient losses. The energy density is now calculated in the cable thermal equilibrium volume as discusses in Section 6.3.

$$\dot{D}_{SS} = Q_{BLM} \cdot P_{QL}/E_D^{cable} \tag{5}$$

The thresholds are expressed as signal rate, but in Table 5 they are also presented for 84-second integration time which is the longest signal-collection interval of the BLM system.

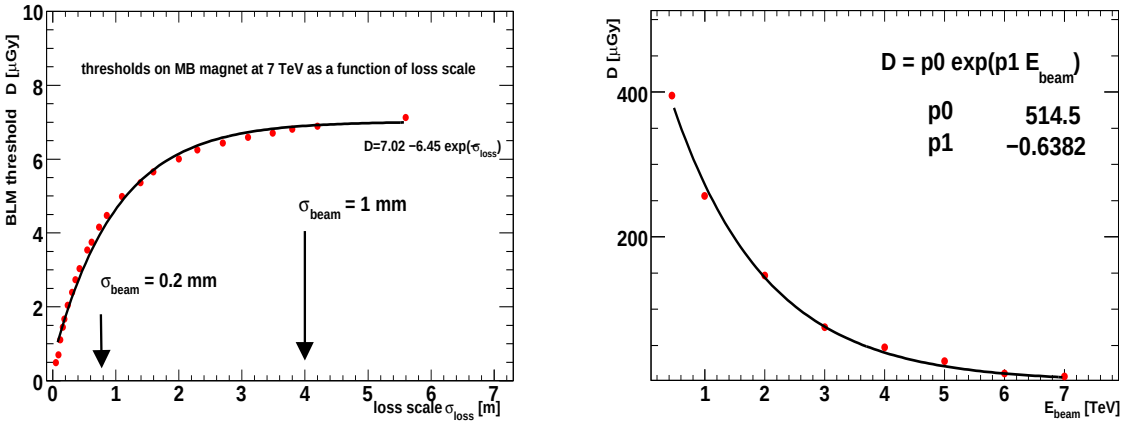

Figure 20: *Left plot: illustration of the dependency of the threshold value at collision energy from the scale of the loss distribution. Shrinking the transverse beam size from 1 to 0.2 mm leads to thresholds decrease by 50%. Fitting the dependency with assymptotic functions give values between 7 and 8 μGy for losses distributed over a distance more then 4 meters. Right plot: threshold on the MB magnet as a function of the beam energy.*

The total dose, as seen by the Beam Loss monitors, which correspond to magnet quench for Steady State loss is 5 to $8 \cdot 10^3$ times higher then the one for transient loss.

8.2 Error estimation

It is assumed that the Q_{BLM} and E_D^{max} are independent parameters and the conversion constant C_{Gy}^C which is calculated from gas ionization energy, is known with a negligible error [27]. Therefore the error of the threshold contains errors of the maximum energy density (E_D), BLM signal (Q_{BLM}) and cable enthalpy (H_{cable}).

$$\left(\frac{\Delta D}{D}\right)^2 = \left(\frac{\delta D}{\delta Q_{BLM}}\right)^2 \Delta Q_{BLM}^2 + \left(\frac{\delta D}{\delta H_{cable}}\right)^2 \Delta H_{cable}^2 + \left(\frac{\delta D}{\delta E_D}\right)^2 \Delta E_D^2 = \tag{6}$$

$$(C_{Gy}^C)^{-2} \left[\left(\frac{H_{cable}}{E_D}\right)^2 \Delta Q_{BLM}^2 + \left(\frac{Q_{BLM}}{E_D}\right)^2 \Delta H_{cable}^2 + \left(\frac{H_{cable} Q_{BLM}}{E_D^2}\right)^2 \Delta E_D^2\right] \tag{7}$$

	horizontal loss				vertical loss			
	beam 1 right		beam 1 left		beam 1		beam 2	
BLM	inj	coll	inj	coll	inj	coll	inj	coll
at 25 cm								
Q_{BLM}[aC/prot]	10.9	279.3	8.8	67.7	8.5	469.4	1.1	39.9
D[μGy]	46.4	1.0	37.5	0.2	146.2	32.3	18.9	2.7
at 75 cm								
Q_{BLM}[aC/prot]	21.6	711.2	22.0	210.0	19.7	833.8	3.2	83.1
D[μGy]	92.0	2.4	93.7	0.7	338.9	57.5	55.1	5.7
at 125 cm								
Q_{BLM}[aC/prot]	22.8	734.0	21.9	212.6	19.0	679.9	3.3	89.2
D[μGy]	97.1	2.5	93.2	0.7	326.9	46.8	56.8	6.1
at 175 cm								
Q_{BLM}[aC/prot]	18.8	507.7	14.7	155.7	14.7	559.8	2.8	82.5
D[μGy]	80.1	1.7	62.6	0.5	252.9	38.6	48.2	5.7
at 225 cm								
Q_{BLM}[aC/prot]	11.8	302.7	9.2	110.4	10.9	425.9	2.4	71.3
D[μGy]	50.3	1.0	39.2	0.4	187.5	29.3	41.3	4.9
at 475 cm								
Q_{BLM}[aC/prot]	3.7	83.9	3.6	35.4	2.9	85.0	0.7	14.7
D[μGy]	15.8	0.9	15.1	0.1	49.9	5.9	12.0	1.0
Distributed losses								
Q_{BLM}[aC/prot]	6.2	145.5	5.0	50.8	5.1	190.3	1.0	24.6
D[μGy]	492	19.8	395	6.9	1394	154	266	19.9

Table 4: *Signals in BLMs corresponding to single lost proton (Q_{BLM}) and to quench level for fast losses (D). The values of the maximum energy density in the coil is from Table 2. The most conservative enthalpy limits of the cables are chosen in procedure of threshold determination.*

The difference between the results of cable enthalpy limit estimation from [6] and [18] vary from 10% at injection energy to more than 100% at collision energy. But the relative error in case of the most pessimistic estimations used here is 20% [26] and this error is used in the error analysis.

The error of the estimation of the maximum energy deposition (ΔE_D) in the coil is described earlier. The limited MC sample gives about 5% of statistical error. The accuracy of procedure of determining the maximum value from the radial distribution of energy deposit varies from 10% at injection and 20% at collision energies. The accuracy of the Geant4 model itself is very good for energy deposit, therefore it is neglected. The overall $\Delta E_D/E_D$ is 11% at injection and 21% at collision energy.

The estimation of the error of the BLM signal (ΔQ) is more complex. From [15] the estimated accuracy of the Geant4 cascade tail simulation is about 20%. The

	horizontal loss (right beam)		vertical loss	
	injection	collision	injection	collision
max pointlike				
$\dot{D}$ [Gy/s]	$5.57 \cdot 10^{-3}$	$2.03 \cdot 10^{-4}$	$1.08 \cdot 10^{-2}$	$4.40 \cdot 10^{-4}$
D [Gy](84 s)	0.47	0.017	0.907	0.037
distributed				
$\dot{D}$ [Gy/s]	$3.02 \cdot 10^{-2}$	$1.77 \cdot 10^{-3}$	$3.56 \cdot 10^{-2}$	$6.77 \cdot 10^{-3}$
D [μGy](84s)	2.54	0.149	3.00	0.568

Table 5: *Estimated thresholds for Steady State losses.*

5% error is coming from Monte Carlo statistics. The reproduction of the response function gives and the algorithm to retrieve the signal give all together the error of about 20%.

Taking into account the error sources it is find that the quench-protecting thresholds in the Beam Loss monitors are determined with error of about 40%. The contributions to the uncertainty from different terms is summarized in Table 6. The uncertainty of the estimation of the BLM signal due to single proton impact is the most important source of error.

E_{beam}	contribution from ΔQ_{BLM}	contribution from ΔH_{cable}	contribution from ΔE_D	total error
450 GeV	29%	20%	11%	37%
7 TeV	29%	20%	21%	41%

Table 6: *Contribution of various error sources to the total error of quench-protecting threshold estimation.*

9 First quench of LHC magnet with beam

The first LHC injection test took place during the weekend starting on August 8th, 2008. During this test a quench of the Main Dipole magnet (MBB in cell 8L3) has been observed. It took place on the August 9th at 2:19:51 am (local time [7]).

Due to the direct beam impact, the magnet drifted off the superconducting state but recovered by itself. The Quench Protection System (QPS) has been triggered and the magnet was quenched by its quench heaters about 200 ms after the recovery. Therefore the quench took place very close to the coil stability margin and can be used to calibrate the BLM system.

The quench took place during the procedure of aperture scan in which an increase of the transverse beam oscillations has been induced. Three consecutive injections of a pilot bunch with $4 \cdot 10^9$ protons were performed. The third injection led to the quench event. The beam position read on the last BPM, placed on the Q8 quadrupole about 25 meters before the quenched magnet was about +10 mm and the beam direction was upward.

parameter	1st quench	2nd quench
UTC timestamp	2008-08-09 00:19:51	2008-09-07 15:34:05
quenched magnet	MB.B8L3	MB.B10R2
beam energy [TeV]	0.45	0.45
number of protons	$4 \cdot 10^9$	$2 \cdot 10^9$
impacting angle	$260 - 300$ μrad	750 murad
loss duration	transient	transient
emmitance ϵ	≈ 0.4mm	≈ 0.4mm
lattice function β		
σ_{beam}	≈ 1 mm	≈ 1 mm
kicking magnet	MCBV.9R2.B1	MCBV.9R2.B1
dcum [m]	3680.22	3680.22
beam position at last BPM [mm]	+10 vertical	-
dcum of loss	6388	3703

Table 7: *Beam parameters during the first and the second quench event.*

Unfortunately, there are discrepancies between the model and the BPM readings upstream the quenched magnet, therefore it was not possible to reconstruct precisely the beam trajectory, and the impact angle with MADX [28]. It has been discovered after later on that the polarities of MQTL magnets were inversed, but this effect has also been included when trying to reproduce beam trajectory with MADX. Therefore the impact angle is estimated from the distance between the BPM and the quench location (reconstructed later), assuming that the MQ and MBA magnets, between the BPM and the quenched magnet, had a small influence on the beam trajectory

[7] LHC logging system by default uses UTC time.

(it should be of the order of a few μrad). The distance between the BPM and the quench location is about 27 meters what gives the impact angle between 260 and 300 μrad.

The beam loss monitors on the MBB magnet are placed on the opposite side of the cryostat and they are foreseen to observe losses induced by the collimators upstream the beam 2. The loss duration is in the nanosecond scale, but because of long cabling together with electronics effects which are still being investigated, the total signal is integrated only for time between 0.8 and 10 ms. This effect is illustrated in Figure 21 and Table 8, where the signals used for analysis are marked with a bold font. For 1.3-second integration time the signal is lower because of averaging of the two consecutive acquisitions due to technical reasons. The noise level, measured on the channels after the quench and without the beam, is below 1 μGy.

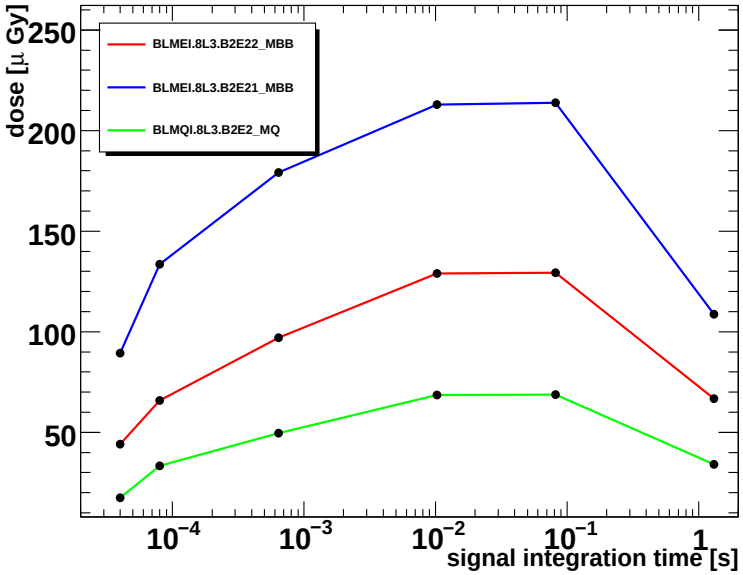

Figure 21: *Total signal integrated for different charge-collection intervals.*

The longitudinal profile of the signal as measured by the Beam Loss Monitors during the quench is presented in Figure 22. The maximum signal is observed in the first monitor on the following MQ magnet due to leak of particles in the interconnection region where there is much less material then in the magnet bulk. The estimated quench level for the monitors placed on the beam 2 is shown with errors as a blue line.

9.1 Comparison with the simulation

The data collected during the quench has been compared with the particle shower simulations, assuming a gaussian transverse profile of the beam. The longitudinal

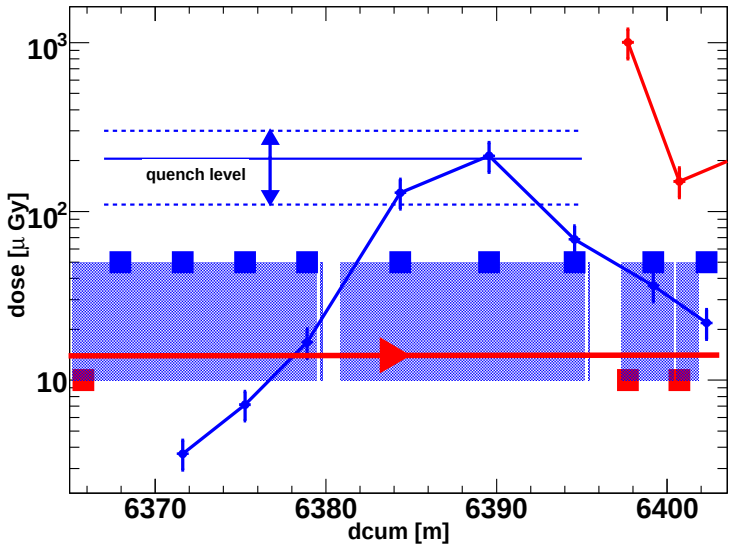

Figure 22: *Signal profile for the first quench of MBB magnet with LHC pilot bunch.*

monitor name	dcum [m]	integrated signal [μGy]			
		40 μs	80 μs	0.64 ms	10.24 ms
BLMEI.8L3.B2E3_MBB	6378.91	3.20	4.63	8.67	**16.81**
BLMEI.8L3.B2E22_MBB	6384.37	44.19	65.74	97.09	**129.05**
BLMEI.8L3.B2E21_MBB	6389.57	89.35	133.62	179.05	**213.15**
BLMQI.7L3.B2E3_MQ	6394.56	17.53	33.43	49.61	**68.31**
BLMQI.7L3.B1I3_MQ	6397.70	112.37	182.15	249.19	249.20

Table 8: *Signals in the BLMs in the area around the quenched magnet. They correspond to UTC time stamp: 2008-09-08, 00:19:51.*

signal profile outside the cryostat fitted with gaussian is presented on the left plot of Figure 23. Fitting with gaussian is approximate and assumes neglecting the tail of the cascade. It is a good approximation in case when the gaussian loss is wider then the length of the cascade.

In the simulation the distribution of the beam impacting on the surface of the beam screen is transformed into the signal in the BLMs using the parametrized dependence from Figure 17 (the blue points on the upper right plot are used). Initial loss distributions with various σ_{loss} has been tested in order to fit to the data. The green curve on the right plot of Figure 23 shows the signal outside the cryostat due to simulated loss distribution of $4 \cdot 10^9$ lost protons with width $\sigma_{\text{loss}} = 3.7$ m along the beam pipe, what correspond to $\sigma_{\text{beam}} = 1$ mm (assuming impact angle of 250μrad). The resulting distribution outside the cryostat has $\sigma = 4.12$ m, which is very close to the value obtaned by fitting the measurements. The maximum value of the distribution is about 60% of the measured one. The agreement in the maximum

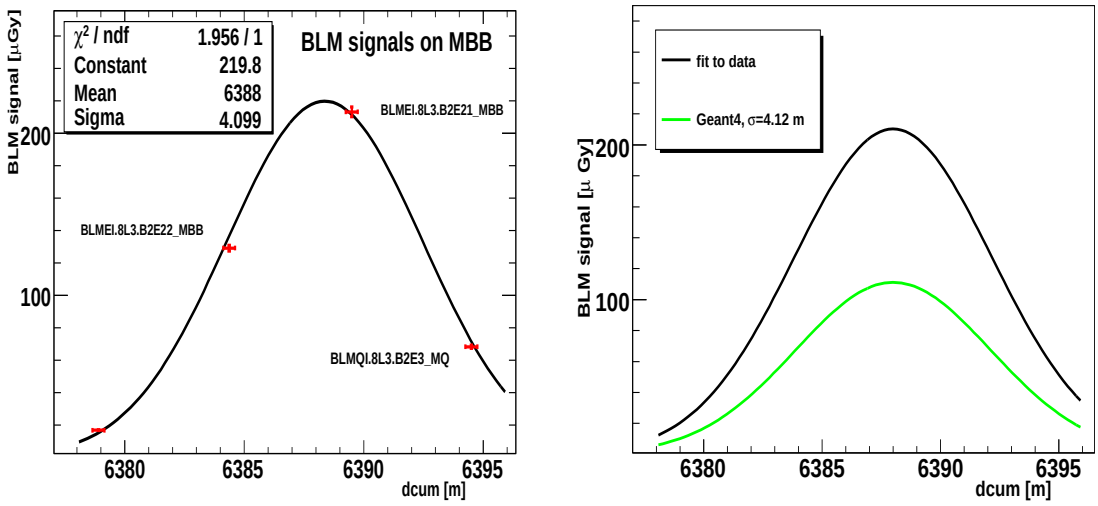

Figure 23: *Left plot: the fit of a gauss curve to the losses measured during the first beam-induced quench of MB magnet. Errors of 1.4% as stated in [25] are used. Right plot: Attempts to obtain the measured signals from Geant4 Monte Carlo simulation of* $4 \cdot 10^9$ *protons distributed along the beam screen with different width. The loss distributions are shown in the next Figure. Monte Carlo procedure cannot reproduce the signal width and the amplitude at the same time.*

can be obtained by reducing the σ_{loss}, but then the width of the distribution does not agree with the measured one. The expected beam size is about 1 mm, therefore the initial loss distribution is expected to be close to $\sigma_{\text{loss}} = 3.7$ m. The back line is a fit to experimental data shown in the left plot.

Assuming the hypothetical loss distributions and using the parametrizations of the maximum energy deposition in the coil $E_D^{\max}$ a reconstruction to enthalphy density limit can be done. The narrower loss distribution (blue line) corresponds to the maximum energy deposit in the coil of 49.9 mJ/cm^3 and the wider one (green) one 13.1 mJ/cm^3, while the theoretical value is about 31 mJ/cm^3.

Following the above argument concerning the initial loss distribution it can be concluded from Figure 23 that the simulation underestimates the signal in the BLMs because it is not possible to obtain the measured signal from the simulation of the loss of the $4 \cdot 10^9$ protons.

It must be stressed that the distribution which fits to the measured width of the signal outside the cryostat is more feasible then the one which fits the peak. It assumes more physical transverse size of the impacting beam (about $\sigma_{beam} = 1\ mm$), and it is also easier to reason the change of the signal amplitude then the signal shape.

10 Second quench of LHC magnet with beam

The second quench took place on September 7th, 2008 at 17:34:05 (local time). The magnet quenched was Main Dipole (MBB) in cell 10R2. The nature of this quench was similar to the first one: the quench precursor has been detected as the voltage drop in the QPS system, a self healing process took place but the QPS heater have been triggered and quenched the magnet. The beam conditions during this event were different then for the first quench.

The deflection angle of 750 μrad has been set on corrector magnet MCBV.9R2.B1 (the same as for the first quench), which is placed about 23 meters from the maximum of the registered signal. As between the corrector magnet and the quenched MB there is no Main Quadrupole, the beam impact angle is equal to deflection angle. The number of protons in the pilot bunch was half of what has been used for the first quench, i.e. $2 \cdot 10^9$.

The signal has been measured by the monitors on correct side of the cryostat, therefore they are almost 6 times higher then in case of the first quench. The Figure 24 shows the event geometry, and the Table 9 shows signal values in the area of interest. The distribution of the signal outside of the cryostat is measured by 6 BLMs (only 3 in case of the first quench) as the monitors are distributed more densely on this magnet. The shape of the distribution is not gaussian anymore as it is expected from larger impact angle (σ_{loss} is not much larger then width of the distribution of BLM signal outside the cryostat) and from the fact that the measurement, in opposition to the first quench, is measured by the monitors on the first beam. Without doubts this quench event is a very good candidate to be compared with the simulations.

monitor name	dcum [m]	integrated signal [μGy]			
		40 μs	80 μs	0.64 ms	10.24 ms
BLMEI.10R2.B1E21_MBB	3701.28	16.20	22.21	27.30	**56.54**
BLMEI.10R2.B1E22_MBB	3703.38	476.68	791.51	1218.09	**1261.02**
BLMEI.10R2.B1E23_MBB	3705.48	211.06	344.12	522.14	**562.20**
BLMEI.10R2.B1E24_MBB	3707.58	75.33	122.21	188.96	**215.63**
BLMEI.10R2.B1E25_MBB	3709.68	39.51	64.48	100.80	**117.27**
BLMEI.10R2.B1E26_MBB	3711.78	21.06	34.13	53.72	**62.79**

Table 9: *Signals in the BLMs in the area around the quenched magnet. They correspond to UTC time stamp: 2008-07-09, 17:34:05.*

On the left plot of Figure 25 the data has been fitted with a Landau curve, similarly to the fit to the simulated signal outside the cryostat. The fit parametrizes the data very accurately.

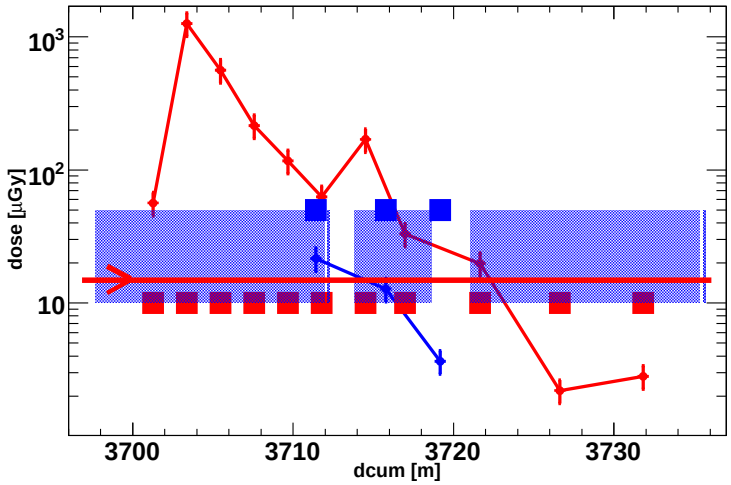

Figure 24: *Signal profile for the second quench of a MBB magnet with LHC pilot bunch.*

A special Geant4 sample with impact angle of 750 μrad has been produced. The energy density distribution inside the coil for this sample is not much different then for standard 250 μrad impact case. The signal outside the cryostat is by about 15% stronger (in maximum), and more narrow (by less then 10%).

The same procedure as in the analysis of the first quench has been used. The Landau signal outside the cryostat due a single proton loss has been folded with gaussian beam loss distribution along the beam screen.

The results of the folding procedure are shown on the right plot of Figure 25. The assumed $\sigma_{\rm loss}$ is only 0.743 m what corresponds to $\sigma_{\rm beam} = 0.9$ mm. The simulated signal is lower then measured one by about 30%. The simulated maximum energy density deposition in the coil is 15.6 mJ/cm^3.

11 Conclusions

The quench protecting thresholds have been determined with Geant4 simulation chain and confronted with the first observed beam-induced quenches of LHC Main Dipole.

In case of transient losses the estimation of the quench-protecting threshold in the Beam Loss Monitors placed on the MB magnet give values of about (395 ± 194) μGy for injection energy and (4.0 ± 2.3) μGy for collision energy. These thresholds assume a loss distribution corresponding to the impact of the beam $\sigma_{\rm beam} = 1$ mm at injection and $\sigma_{\rm beam} = 0.2$ mm at collision. The impact angle is assumed to be 250 μrad. In case of a localized loss, when for instance a limitation of the dynamic aperture occurs, this thresholds should be lowered to about $16 - 100$ μGy for injection energy and

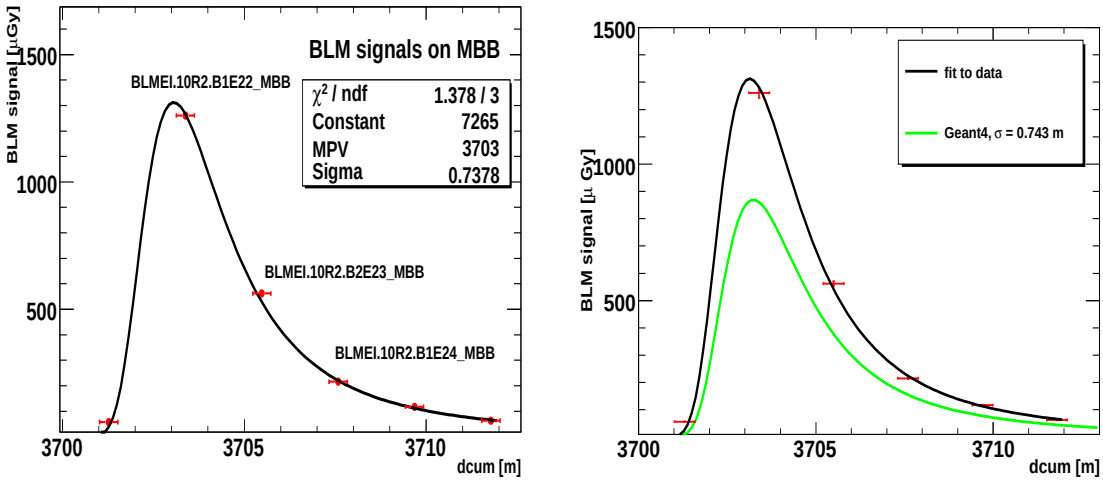

Figure 25: *Left plot: the fit of a landau curve to the losses measured during the second beam-induced quench of MB magnet. Error of 1.4% as suggested in [25] is used.*

$0.3-1.0$ μGy for collision energy depending on the distance between the loss location and the nearest BLM. This numbers does not include additional factor of about 0.5 for thresholds set on integration times between 40 μs and 10 ms due to the time necessary to collect whole signal.

The two beam-induced quenches of the MB magnet which took place in 2008 lead to two main conclusions:

- the signal measured by the BLMs during the quench events is systematically about 30%-50% times higher then estimated by the Geant4 simulation,
- the reconstructed cable enthalpy limit is between 40 and 50% of the calculated one.

The two effects have opposite influence on the threshold value and this is why the numbers shown in Table 4 would protect well the MB magnet from quenching. But this coincidence must be understood by further studies. The underestimation of the BLM signal might be due to error in geometry, but probably it is due to systematic underestimation of fluence of particles in hadronic cascade tail by Geant4 physics models. Additional factor might come from the response functions and the way they are used (see [15]). The last suggestion is supported by the large discrepancy between neutron flux which dominates the low energy part of the spectrum and the neutron contribution to the signal.

An estimation of quench protecting threshold in case of steady-state losses has been made. They give a value of the threshold of 30 mGy/s for injection energy and 1.8 mGy/s at collision. No quenches in steady-state conditions have been observed up to know to verify this estimations.

The relative error of the threshold estimation is about 50%. The largest contribution comes from the signal estimation in the BLMs.

The results presented in this study allow to set safe thresholds to protect MB magnets on LHC as well as give important informations concerning thresholds on other magnets. It is proposed how to analyse quenches in order to validate the thresholds and to obtain informations about the cable enthalpy limits. The thresholds are determined with precision which fulfills the specification requirements but further tests with the beam and simulation improvements are necessary in order to better understand the system and the quench events.

12 Acknowledgments

Authors would like to thank Nikolai Schwerg, David Schiebol and Bernhard Auchmann from Roxie team for discussions and calculations of enthalpy limit for transient losses, Mike Lamont for providing the current levels for MB magnet, Simone Gilardoni and Jorg Wenninger for fruitful discussion and Elena Benedetto for clarifying information concerning the beam conditions during the quench events. Markus Stockner was endlessly patient when asked questions about the response functions and Markus Brugger spend significant amount of time comparying Geant4 and FLUKA results. Stefano Redaelli for carefull reading of the manuscript.

References

[1] LHC Technical Design Report

[2] `http://cern.ch/blm`

[3] P. Bauer, "Stability of Superconducting Strands for Accelerator Magnets", Ph.D. thesis, Technische Universitat Wien, 1998

[4] R. Denz, F. Rodriguez-Mateos, "Electronic system for the protection of superconducting elements in the LHC", EUCAS 2003, LHC Project Report 482

[5] R. Denz et al., "QPS Upgrade and Re-Comissioning", Proceedings of Chamonix Workshop 2009

[6] D. Bocian, EDMS no 750204

[7] J.B. Jeanneret, D. Leroy, L. Oberli, T. Trenkler, "Quench levels and transient beam losses in LHC magnets". LHC Project Report 44.

[8] D. Bocian, B. Dehning, A. Siemko, "Modelling of Quench Limit for Steady State Heat Deposits in LHC Magnets"

[9] P-P. Granieri,"Modelling of cable stability margin for transient perturbations", presentation at THERMOMAG-07

[10] R. Bruce, "Simulation of ion beam losses in LHC magnets", LITH-IFM-EX-05/1514 E

[11] A. Priebe, M.Sapinski, report in preparation

[12] L. Ponce, "Locations of BLM based on proton loss maps", presentation at LHC Collimation WG meeting, June 19th 2006.

[13] L. Ponce, "Locations of BLM based on proton loss maps", a rapport

[14] LHC Collimation WG, private communication

[15] A. Stockner, "Beam Loss Calibration Studies for High Energy Proton Accelerators", PhD thesis 2007

[16] H. Fesefeldt, "GEISHA", RWTH Aachen report PITHA 85/2, 1985

[17] S. Russenschuck, '1st International Roxie Users Meeting and Workshop - ROXIE : routine for the optimization of magnet X-sections, inverse field calculation and coil end design', CERN yellow report 99-01, 1999.

[18] Nikolai Schwerg, priv comm.

[19] E. Wildner, J.B. Jeanneret, "Beam Losses and Collimation in VLHC", presentation at VLHC workshop, February 1999.

[20] Ch. Hoa, F. Cerutti, E. Wildner, "Energy Deposition in the LHC Insertion regions IR1 and IR5", LHC Project Report 1167.

[21] A. Arauzo Garcia, B. Dehning, "Configuration of the Beam Loss Monitors for the LHC arcs", LHC Project Note 238

[22] Data analysis of the BLM test in CERF, 2009, repport in preparation

[23] R.K. Bock et al., "Parameterization of the longitudinal development of hadronic showers", Nucl. Instrum. Meth. Phys. Res. 186 (1981) 533.

[24] Alexander Howard, Gunter Folger, priv. communication

[25] B. Holzer et al. "Development, production and testing of 4500 Beam Loss Monitors", CERN-AB-2008-054

[26] D. Bocian, private comm.

[27] International Commission on Radiation Units and Measurements. "Average energy required to produce an ion pair". ICRU Technical Report 31, Washington D.C., 1979

[28] E. Benedetto, private communication

[29] J. Apostolakis, G. Folger, V. Grichine, A. Howard, V. Ivanchenko, M. Kossov "Hadronic Shower Shape Studies in Geant4", CERN-LCGAPP-2007-02